Deciphering microglial activation and neuronal apoptosis post-traumatic brain injury: The role of TYROBP in inflammation regulation networks

XUDONG ZHOU[1,2], HUIPING SONG[1], JINGJING HE[1], WEI HAN[2] and QIN LI[1,2]

[1]The First Clinical College, Shandong University of Traditional Chinese Medicine, Jinan, Shandong 250355; [2]Emergency Department, Shenzhen University General Hospital, Shenzhen University, Shenzhen, Guangdong 518060, P.R. China

Received November 30, 2023; Accepted February 1, 2024

DOI: 10.3892/mmr.2024.13228

Abstract. Traumatic Brain Injury (TBI) represents a significant public health challenge. Recovery from brain injury necessitates the collaborative efforts of various resident neural cells, predominantly microglia. The present study analyzed rat and mouse RNA expression micro-arrays, high-throughput RNA sequencing and single-cell sequencing data sourced from public databases. To construct an inflammation regulation network around TYRO protein tyrosine kinase-binding protein (TYROBP), to evaluate the role of TYROBP in cell death after TBI. These findings indicate that following TBI, neurons predominantly communicate with one another through the CXC chemokine ligand (CXCL) and CC chemokine ligand (CCL) signaling pathways, employing a paracrine mechanism to activate microglia. These activated microglia intensify the pathological progression of brain injury by releasing factors such as tumor necrosis factor α (TNF-α), vascular endothelial growth factor and transforming growth factor β via the NF-κB pathway. Cells co-culture experiments demonstrated that neurons, impaired by mechanical injury, interact with microglia through non-contact mechanisms. Activated microglia secrete cytokines, including TNF-α, CXCL-8 and CCL2, which trigger an inflammatory response and facilitate neuronal apoptosis. TYROBP gene knockout in microglia was demonstrated to reduce this interaction and reduce neuronal cell apoptosis rates.

Correspondence to: Professor Qin Li, The First Clinical College, Shandong University of Traditional Chinese Medicine, 4655 University Road, University Science Park, Changqing, Jinan, Shandong 250355, P.R. China
E-mail: liqin701015@163.com

Key words: TYRO protein tyrosine kinase-binding protein, microglia, traumatic brain injury, neuronal cell death, NF-κB pathway, inflammatory response

Introduction

Traumatic brain injury (TBI), often termed the 'silent epidemic' presents significant health challenges due to its overlooked nature and severe repercussions. Annually, TBI results in disability for 6-10 million individuals, globally, with ~60% of survivors developing neurological or psychiatric disorders (1). This leads to substantial psychological distress and societal and familial burdens (2). TBI can directly impair brain tissue, with neuronal injuries and cell death impacting nerve conduction and leading to cognitive deficits such as impaired memory and attention (3). Additionally, vascular damage and blood supply issues can further exacerbate brain tissue damage (4). Notably, after injury, inflammatory response imbalances can aggravate neuronal damage and hinder the repair process, potentially resulting in long-term functional deficits (5). Psychological conditions, including depression and anxiety, are also frequent among TBI patients (6).

The pathophysiology of TBI is multifaceted, encompassing various cellular and sub-cellular events, such as trauma response, inflammation, damaged area clearance, neural stem cell activation, synaptic remodeling and angiogenesis. A crucial factor in TBI prognosis is the role of glial cells, particularly microglia. Microglia can phagocytose and break down damaged cells and neuron fragments to clear the damaged area and maintain neuroglial homeostasis and neurovascular integrity. However, prolonged and excessive microglial activation can harm adjacent healthy neurons. The excessive release of cytokines and chemical mediators during an overactive inflammatory response can further harm brain tissue, creating an 'inflammatory storm' that exacerbates brain damage (7,8). When microglia are activated, they can release neurotoxic chemicals such as reactive oxygen species, nitric oxide, cyclooxygenase and excitatory amino acids. These chemicals can exacerbate neuronal damage or dysfunction, and cell death (9,10).

Transmembrane DNAX-activation protein 12, also known as TYRO protein tyrosine kinase-binding protein (TYROBP), serves an important role in the control of inflammatory responses and is responsible for maintaining a stable neural micro-environment and preventing neuron death. TYROBP is mostly found in immune cells and neurons. It is

an adapter protein which modulates immune receptor signal transduction which effects how immune cells and neurons are activated (11,12). For instance, previous studies have reported that the abnormal expression of TYROBP in neurodegenerative diseases, such as Alzheimer's and Parkinson's disease may relate to disease development and progression (13,14). TYROBP is also linked to autoimmune encephalitis and other neuro-immunological diseases. However, the precise role and mechanism of TYROBP in TBI remains unclear, with research presenting contradictory results, possibly due to factors like different experimental models and sample sizes, and disease complexity (15). The function of TYROBP may also vary across cell types and neurological conditions, complicating research interpretations. Further investigation of the role of TYROBP is essential for understanding neurodegenerative diseases and inflammatory responses in brain injuries and is crucial for developing novel therapies, advancing personalized medicine and overcoming current research limitations.

The present study aims to explore the mechanisms of the neuroinflammatory response induced by TBI and to investigate potential therapeutic targets. To elucidate the mechanisms of the role of TYROBP following TBI, the bioinformatics analysis identified key signaling nodes centered around TYROBP. These nodes make up a regulatory network that has an impact on neuronal ferroptosis, apoptosis and autophagy. After TBI, neurons engage in paracrine secretion through the CXCL and CCL signaling pathways, activating microglia. These activated microglia can worsen brain injury pathology by releasing TNF-a, VEGF and transforming growth factor β (TGF-β) via the NF-κB pathway. Inhibiting the TYROBP gene in microglia can decrease this interaction and lower neuron mortality rates. The present study underscores the role of TYROBP in TBI and offers novel insights into therapeutic approaches targeting microglial cells.

Materials and methods

Data sorting and differential analysis. TBI-related RNA expression profiling micro-arrays and high-throughput sequencing datasets were sourced from the Gene Expression Omnibus (GEO) database (https://www.ncbi.nlm.nih.gov/geo). The selection criterion mandated the use of a mouse model developed via the controlled cortical impact method, which mimics brain injuries from impacts or blows similar to those in accidents, traffic collisions, falls and sports injuries (16). Studies involving controlled impacts to the cerebral cortex under craniotomy conditions, employing mechanical, hydraulic or free-fall shocks, were included. Other modeling techniques; such as, closed-skull impact and puncture methods, were excluded. The control group comprised mice subjected to sham surgery involving craniotomies without brain injury impacts.

Sequencing data was processed on the R project platform (https://cloud.r-project.org; version 4.3.2). The 'ComBat' function from the 'Surrogate Variable Analysis' package was used for dataset integration and batch effect elimination (17). Samples were normalized using the 'normalizeBetweenArrays' function. Differential analysis was performed using the 'DESeq2' package, with $P<0.05$ and log fold change (logFC) >0.5 as significance thresholds. After batch effect removal, the two microarray datasets were analyzed using the 'limma' package (18). Heat maps were generated via the 'pheatmap' function from the 'ComplexHeatmap' packages and volcano maps were created using tools available on the Chiplot website (https://www.chiplot.online).

Enrichment analysis. Differentially expressed genes related to TBI from both sequencing and microarray datasets were imported into MetaScape (https://metascape.org, version 2022-10-01) for comprehensive enrichment analysis (19). This involved pathway and process enrichment analysis using ontology sources, including the Kyoto Encyclopedia of Genes and Genomes (KEGG) pathway, Gene Ontology (GO) Biological Processes, Reactome Gene Sets, Canonical Pathways, Comprehensive Resource of Mammalian protein complexes (CORUM), WikiPathways and Protein Analysis Through Evolutionary Relationships (PANTHER). Analysis was focused on clusters of terms with $P<0.01$, a minimum count of 3 and an enrichment factor >1.5, based on shared characteristics and membership similarities.

For enhanced insight into term relationships, a subset of enriched terms was selected and represented in a network plot generated by MetaScape, highlighting the complex interactions among them. Terms with a similarity score >0.3 were connected.

Subsequently, to further investigate the protein-protein interaction (PPI) within these terms, databases such as Search Tool for the Retrieval of Interacting Genes/Proteins (STRING, https://cn.string-db.org/), BioGrid (https://thebiogrid.org), OmnIPath (https://github.com/saezlab/Omnipath_Cytoscape) and InWeb IM (http://www.intomics.com/inbio/map) were used. This process produced a network visualizing the interconnectedness of proteins and the Molecular Complex Detection (MCODE) algorithm was applied to identify and emphasize densely interconnected network components.

Immune infiltration score. RNA sequencing data was converted into Transcripts Per Million (TPM) format for streamlined analysis. The 'CIBERSORT' package in R was used to analyze the types and proportions of immune cell infiltration in brain tissue. For data visualization, the 'ggpubr' package was used. The degree of immune infiltration of each sample was assessed using the Estimation of Stromal and Immune cells in Malignant Tumours using Expression data (ESTIMATE) score.

The sequencing dataset was classified into two main groups based on treatment, the TBI group and the Sham operation group. The dataset was further divided based on detection time after treatment, resulting in three distinct time-frames, 1 week, 1 month and 3 months. Additionally, the data was categorized by tissue type, including the cortex, thalamus, hypothalamus and hippocampus. Statistical significance between these groups was determined using unpaired Student's t-test.

Weighted gene co-expression network analysis (WGCNA). Inflammatory responses following brain trauma involve multiple immune-related genes. WGCNA was used to find the gene group that was most linked to neuroinflammation after brain injury and to explain key immune mechanisms (20).

The 'WGCNA' package in R was used to load and clean the data, remove missing values, outliers and duplicates, compare visual phenotypic data with gene expression data, build a sample clustering tree, create a network and find modules, chose the correct soft threshold and average connectivity, linked modules to phenotypic data, and identify the gene set most relevant to the immune response.

The 'blockwiseModules' function in WGCNA was used for efficient network construction and module detection in large gene datasets. To identify the genes important for immune regulation for TBI, a PPI network was constructed from the gene set that WGCNA identified in the STRING database, the interaction score requirement was set to high confidence, selecting key genes with a node degree ≥5 for further cluster analysis.

Cell death. From the GSEA database (https://www.gsea-msigdb.org) we selected five gene sets related to cell death, including apoptosis (ALCALA_APOPTOSIS.v2022.1.Hs), necrosis (GOBP_NECROSIS.v2022.1.Hs), autophagy (GOBP_AUTOPHAGY.v2022.1.Hs), ferroptosis (WP_FERROPTOSIS.v2022.1.Hs) and pyroptosis (GOBP_PYROPTOSIS.v2022.1.Hs). These selections were informed by validated literature and expert insights. In the present analysis of experimental data using GSEA software, gene sets demonstrating statistically significant enrichment were focused on, thus ensuring the scientific integrity and quality of the selection process.

Using the different levels of expression of these gene sets in the sequencing data, five different cell death scores after TBI were assigned. These scores compared the extent and type of cell death between the Sham and TBI groups. Additionally, the TBI group samples were subdivided by detection time and tissue type for comparative analysis using cell death scores. Unpaired Student's t-test was used to assess the statistical significance of differences across these groups.

Cluster analysis. The aim of the cluster analysis was to divide TBI samples into groups based on the immune-related gene set that was found, allowing a link between immune-related genes and cell death scores to be established. This analysis employed the 'ConsensusClusterPlus' package (21) on the R project platform.

Firstly, the gene matrix was normalized then the 'ConsensusClusterPlus' function was used for consistent clustering. This process included constructing cluster consensus and item-consensus matrices, followed by generating visual representations of these matrices.

In the final step, a box plot to represent different groups and their respective cell death modes was created. Unpaired Student's t-test was used to evaluate statistical significance in variations in cell death among these groups.

Single-cell sequencing analysis. Three single-cell sequencing datasets relevant to TBI (GSE180862, GSE160763 and GSE101901) were downloaded from the GEO database. These datasets underwent quality control, adhering to the specific criteria that feature RNA (count) must be >200 but <2,500, and mitochondrial content must be <5%.

These datasets were combined using the 'merge' function, then the Harmony method (https://github.com/immunogenomics/harmony; version 1.2.0) was applied to reduce batch effects. For dimensionality reduction, the t-distributed stochastic neighbor embedding (tSNE) method was used. The 'monocle2' package (22) was used to create a time-series analysis of microglia in the TBI group to better understand the role of microglia subgroups in TBI.

This approach to comparing expression differences among various cell clusters in single-cell data included conducting gene set variation analysis (GSVA). The RNA of all cells in each cluster was averaged using the 'AverageExpression' package, representing the gene expression profile for each cluster. Subsequently, GSVA was then used to explore variations in biological processes among clusters, with results presented as heat maps. Using the 'plot_genes_in_pseudotime' function, gene expression pseudotime plots were also made to assess the role of immune cell surface activating receptors after TBI.

The remaining data sorting procedures followed the standard protocol of the 'Seurat' package (23). The 'FeaturePlot' function was used to generate visual charts that integrated single-cell expression profiles with Uniform Manifold Approximation and Projection (UMAP), which provided a clear display of the expression of the genes of interest in various cell types. Conversely, the 'VlnPlot' function presented a quantitative view of gene expression in each cell type, enabling more effective comparisons.

The seven key immune node genes previously identified with WGCNA and the STRING database are crucial in the pathology of TBI. It is vital to locate and analyze them at the cellular level. The 'FeaturePlot' function was applied to illustrate the distribution of key immune node genes across cells and the 'VlnPlot' function was applied to create a violin plot of key node gene distribution differences.

GSVA was used to evaluate gene expression differences between the Sham and TBI groups. This was followed by enrichment analysis using the KEGG dataset.

Finally, the 'SCENIC' package was employed to identify transcription factors that regulate gene expression changes in brain tissue following TBI, uncovering key roles and mechanisms.

Cell-cell communication analysis. For the cell communication analysis, the 'CellChat' package (24) on the R project platform was used. The sorted single-cell data was classified into two groups, the Sham group and the TBI group. From these, the gene expression matrix and meta data were extracted. The 'createCellChat' function was then used to construct the CellChat object for further analysis.

After loading the CellChatDB-mouse database (http://www.cellchat.org), the 'Secret Signaling' sub-database was used to study intercellular communication. The established CellChat procedure was followed for subsequent steps. To facilitate comprehensive analysis, the 'mergeCellChat' function was employed to consolidate the two CellChat datasets.

Furthermore, the 'compareInteractions' function was used to evaluate the quantity and intensity of interactions between the Sham and TBI group. The changes in communication between innate immune cells and central nervous system cells

were highlighted. The 'RankNet' function, a ranking-based neural network model, was used to compare intercellular communication pathways between the Sham and TBI groups. This method allowed the identification and quantification of differences in signaling dynamics between the two groups, showcasing the effects of TBI on cellular communication. The 'NetVisual_diffInteraction' function was used to demonstrate the differences in cell communication in the TBI group compared with the Sham group.

To provide a detailed view of the inferred intercellular communication network for each signaling pathway or ligand-receptor pair, a hierarchy plot was made using the 'netVisual_individual' function. Here the directional and strength changes in CCL pathway signal transduction were analyzed. The 'identifyCommunicationPatterns' function was applied to understand how certain cell populations and signaling pathways interacted.

In the present study, the 'netAnalysis_river' function was utilized to create a Sankey diagram that provided a visually intuitive representation of the data, illustrating the associations and interactions among genes within different cell groups and how these contribute to the overall communication network in the datasets of the TBI group.

Mechanical injury method to establish an in vitro TBI model. To model TBI *in vitro*, two distinct co-culture systems were developed, a non-contact co-culture, designed to assess microglial cell activation, and a contact co-culture system, aimed at evaluating neuronal cell survival. These systems allowed the assessment of microglial cell activation states and neuronal cell apoptosis ratios. In the non-contact system, RAW264.7 cells, a type of mouse mononuclear macrophage leukemia cell, can mimic the polarization, phagocytosis, and cytokine secretion functions of various macrophage subtypes, including microglia. (cat. no. CL-0481; Procell Life Science & Technology Co., Ltd.), and PC12 cells, which are rat pheochromocytoma cells of the adrenal gland capable of differentiating into neuron-like cells (cat. no. CL-0190; Procell Life Science & Technology Co., Ltd.), were cultured in a Transwell culture dish. The cells were arranged in a 1:5 ratio with RAW264.7 cells on the lower layer and PC12 cells on the upper layer, separated by a polycarbonate membrane with 3 μm pores. Conversely, the contact co-culture system involved directly mixing the two cell types in a 1:5 ratio and seeding them together in the culture dish. Cells were cultured in high-glucose DMEM medium (cat. no. SH30023; Univ-Bio, Inc.), supplemented with 1% penicillin, 1% streptomycin and 10% fetal bovine serum (cat. no. SH30406; Univ-Bio, Inc.), and incubated at 37˚C in a 5% CO_2 environment for 24 h to promote adhesion and growth.

In order to create a TBI cell model after growth, the mechanical injury model as previously described by Liu *et al* (25) was used. This involved mechanically injuring the PC12 cells to trigger activation in the RAW264.7 cells. Specifically, sterile pipette tips (0.5-10 μl; cat. no. 4901; Corning, Inc.) were used to scratch the PC12 cells manually, 11 scratches per 6-well culture dish were made, forming a grid measuring 3x3mm. During this process, the culture medium was not changed. Cells without scratches served as controls. The dishes were then returned to the incubator for further cultivation.

After 24 h, RAW264.7 cells were collected from a non-contact co-culture by aspirating the medium, detaching them with 0.25% trypsin-EDTA (cat. no. 25200056), neutralizing with serum-rich medium, centrifuging at 300 x g for 5 min at 4˚C and resuspending the pellet for analysis. In the contact co-culture system, the initial step involved treating the culture medium with a low concentration of trypsin-EDTA (0.05%; cat. no. 25300054) for 1 min. This procedure aimed to selectively detach the more loosely adherent PC12 cells, facilitating their separation from the co-cultured cells with minimal disruption.

Cell experiments and grouping. Cells were grouped into five different treatment groups as follows: The natural control group (NC group); the TBI model group (TBI group); the empty plasmid (EMP group) group; the TYROBP gene knockout group (TYROBP group) and the negative control group (TPCA1 group). TPCA-1, is a highly effective and selective IKK-2 inhibitor, which inhibits IKK-2, a key kinase in activating NF-κB. This inhibition is important for controlling inflammatory and immune responses (26). In the NC group, cells were cultured in an ideal environment without any mechanical damage to the PC12 cells. The TBI group used mechanical cutting to establish the TBI model. In the non-contact co-culture system, only the underlying PC12 cells were mechanically damaged, whereas in the contact co-culture system, both cell types were subjected to mechanical damage. For the TYROBP group, RAW264.7 cells, in which the TYROBP gene had been knocked out using CRISPR-Cas technology, were used alongside the same PC12 cell line. The EMP group, serving as a control, used RAW264.7 cells transfected with an empty plasmid.

Gene knockout. The knockout of the TYROBP gene was performed using plasmids (TYROBP-KO guide RNA (gRNA) in pCRISPR-Cas9-U6-gRNA-CMV-Cas9-2A-Puro-RFP Vector; target sequence: 100 ACGGAAGAACAGTCGCATCT; TYROBP-Exon-1, corresponds to the ITAM domain) purchased from Applied Biological Materials Inc (cat. no. 48895114). Any empty vector control (EMP) group, using a blank plasmid with Cas9 and non-specific gRNA was used as a control. RAW264.7 cells in the logarithmic growth phase were cultured in a 12-well plate. When cell density reached 70-80%, the complete culture medium was replaced with serum-free culture medium. Mixed plasmids, including three different genomic DNA constructs designed for specific gene targeting, were transfected into the RAW264.7 cells using Lipofectamine 3000 (cat. no. L3000015; Thermo Fisher Scientific, Inc.) according to the manufacturer's instructions, and after a series of subsequent screenings, the plasmid that demonstrated the most effective gene modulation was selected for further experimentation. The transfection status was assessed under a fluorescence microscope 24 h after transfection. To isolate single clone cell strains with the TYROBP gene knockout, the culture medium was supplemented with 1.0 mg/l puromycin.

qPCR analysis demonstrated a 91% reduction in TYROBP mRNA levels following gene knockout and western blotting

demonstrated a marked decrease in TYROBP protein expression levels, these results indicated the substantial and specific effect of the gene knockout. In the EMP group, TYROBP mRNA and protein levels demonstrated no apparent difference compared to the untransfected negative control (NC), which indicated that the transfection process alone had no effect on TYROBP expression.

Reverse transcription-quantitative polymerase chain reaction (RT-qPCR). Total RNA of RAW264.7 cells was extracted using TRIzol® reagent (cat. no. 15596026; Thermo Fisher Scientific, Inc.) and reverse-transcribed into cDNA using the BeyoRT TM III First Strand cDNA Synthesis Kit. The experiment was conducted according to the manufacturer's protocol. qPCR was performed using a real-time fluorescence quantitative PCR instrument (QuantStudio™ 5 Dx; Thermo Fisher Scientific, Inc.) and the PowerUPTM SYBRTM Green Master Mix kit (Thermo Fisher Scientific, Inc.; cat. no. A25743). The PCR reaction system was 10 μl in total, including 4 μl cDNA, 5 μl SYBR Green Mix and 0.5 μl of each primer. The PCR conditions were as follows: Initial heating at 50˚C for 2 min then initial denaturation at 95˚C for 2 min; followed by 40 cycles of denaturation at 95˚C for 15 sec, annealing at 60˚C for 1 min, and extension at 72˚C for 30 sec. mRNA levels were quantified using the $2^{-\Delta\Delta Cq}$ method (27) and normalized to GAPDH, which was used as the internal reference gene. The primer sequences for qPCR were obtained from the PrimerBank database (https://pga.mgh.harvard.edu/primerbank) and validated in experiments (Table SI).

Western blotting. After 24 h of co-culture, RAW264.7 cells were collected from the Transwell chamber and total proteins were extracted using RIPA lysis buffer (Thermo Fisher Scientific, Inc.; cat. no. 89900). Proteins were separated by SDS-PAGE and transferred onto a PVDF membrane, which were then incubated with primary antibodies for NF-kB p65 (1:700; Affinity Biosciences; cat. no. AF5006), Phospho-NF-kB p65 Ser536 (1:500; Affinity Biosciences; cat. no. AF2006), TYROBP (1:1,000; Abcam; cat. no. ab280568) and GAPDH (1:500; Affinity Biosciences; cat. no. AF7021) overnight at 4˚C. The membrane was then treated with a horseradish peroxidase-conjugated secondary antibody (1:1,000; Affinity Biosciences; cat. no. S0001) for 2 h at room temperature. After washing with PBS, the membrane was developed in an X-ray film cassette, and the films were scanned and analyzed using QuantityOne software (version 4.6.8; Bio-Rad Laboratories, Inc.). GAPDH was used as the loading control for normalizing target protein expression. Each experiment was performed in triplicate.

Immunofluorescence. RAW264.7 cells from the Transwell chamber were fixed in a chilled methanol-acetone mixture (1:1; 4˚C; 1 h) and permeabilized with a 0.5% Triton X-100/PBS solution. After rinsing, the cells were incubated overnight at 4˚C with NF-κB primary antibodies (1:1,000; Affinity Biosciences; cat. no. AF5006). The cells were washed with PBS, then treated with an Alexa Fluor® 488-conjugated secondary antibody (1:100; Abcam; cat. no. ab150077) at room temperature for 1 h. DAPI was used for nuclear staining and incubated with the cells for 5 min at room temperature. Finally, an anti-fade mounting agent (Beijing Solarbio Science & Technology; cat. no. S2100) was added and images were captured using a fluorescence microscope.

Enzyme-linked immunosorbent assay (ELISA). Following the co-cultivation of RAW264.7 and PC12 cells, the cell culture supernatant was collected and centrifuged (4˚C; 300 x g; 10 min) to remove cell debris. The resulting supernatant samples were diluted and used directly for the ELISA assays of TNF-α, CXCL8 and CCL2 using Mouse SimpleStep ELISA® kits (Abcam; cat. nos. ab208348, ab46032 and ab100777). Freshly prepared, diluted standards for each protein were used in each experiment. Standards and samples were added to the antibody-pre-coated micro-plate wells, followed by the introduction of the corresponding antibody cocktail, and incubated at room temperature. Several washing steps were performed to remove unbound materials. Next, 3,3',5,5'-Tetramethylbenzidine (TMB) substrate was added, and the mixture was incubated in darkness. The reaction was stopped with Stop Solution, and the absorbance was measured using a micro-plate reader. A standard curve, generated from the absorbance of the standards, was used to determine the concentrations of TNF-α, CXCL8 and CCL2 in the samples. All experiments were duplicated to ensure data reliability and consistency. Protein expression levels were calculated, with each experiment independently replicated six times. All experiments were conducted strictly according to the manufacturer's instructions.

Cell counting assay. A Cell Counting Kit-8 (CCK-8) assay (cat. no. E-CK-A362; Elabscience Biotechnology, Inc.) was used to measure the survival rate of neuronal cells after a TBI. PC12 cells and RAW264.7 cells were co-cultured in a 5:1 ratio in a 96-well plate, with each well containing $5x10^3$ cells. Cells were incubated for 24 h, then a mechanical transection method was used to mimic TBI, and the cells cultured for 24 h (37˚C; 5% CO_2). Then, 10 μl of CCK-8 solution was added to each well and incubated for 1 h at 37˚C. Absorbance (OD) at 450 nm was measured using a Thermo Fisher Scientific, Inc. micro-plate reader. The average OD of six control wells was used as the reference for 100% cell survival. Blank wells (with culture medium but no cells) were also included as a control. Cell viability was calculated as follows: (sample OD-blank OD/control OD-blank OD) x 100. Each experiment was independently replicated six times.

Annexin V/PI cell apoptosis assay. The annexin V/PI cell apoptosis assay uses the combination of annexin V and Propidium Iodide (PI) for staining, which distinguishes between apoptotic and necrotic cells in a cell population. The FITC Annexin V Apoptosis Detection Kit I (cat. no. 556547; BD Biosciences) was used according to the manufacturer's instructions. Briefly, PC12 and RAW264.7 cells were harvested after 24 h of co-culture, the medium from six-well plates was discarded and the cells washed thrice with cold 1X PBS, then the cells were resuspended and a suspension of one million cells in 100 μl 1X binding buffer was prepared. A total of 5 μl each of annexin V and PI was added to the suspension, followed by a 30 min incubation in the dark at room temperature

before the suspension volume was adjusted to 500 μl with 1X binding buffer. Analysis was performed within 1 h using BD FACSCalibur™ Flow Cytometer (BD Biosciences), ensuring the cells remained in the dark until assessment. Data were processed using FlowJo (version 10.8.1; Becton, Dickinson and Company). Untreated cells were identified on the Forward Scatter-Side Scatter plot, and the proportion of cells in each quadrant was calculated.

Statistical analysis. Data analysis and graph plotting were performed using GraphPad 9.0 software (Dotmatics). All experiments were independently repeated six times. Quantitative data, adhering to a normal distribution, were expressed as mean ± standard deviation. Comparisons between two groups were performed using an unpaired t-test, while multiple group comparisons were performed with one-way ANOVA, followed by post hoc pairwise comparisons with the Bonferroni test. $P<0.05$ was considered to indicate a statistically significant difference.

Results

Data sorting and difference analysis. Eight RNA sequencing datasets (GSE192979, GSE173975, GSE167459, GSE163415, GSE173431, GSE144193, GSE129927 and GSE79441) and two microarray datasets (GSE180811 and GSE71846) (Table SII) were converted to a count format for differential analysis. Batch effects arising from differences in experimental conditions lead to variations in total RNA expression levels among different samples in the original data, making direct comparisons between datasets challenging (Fig. 1A). After applying standardization techniques, the total expression levels across all samples became uniform, eliminating disparities and enabling accurate comparisons (Fig. 1B). The purpose of this correction was to ensure that subsequent analyses accurately reflected true biological differences between samples, eliminating biases introduced by experimental variability.

Differential analysis using the 'DESeq2' package identified 103 differentially expressed genes in the RNA sequencing datasets, with 40 genes down-regulated and 63 up-regulated after brain trauma. A notable difference in gene expression was demonstrated in CCL13, TREM1, CXCL2 and SELE between the Sham and TBI groups (Fig. 1C and D).

Analysis of the two microarray datasets using the 'limma' package identified 135 differentially expressed genes. The top 10 genes have already been displayed such as PPBP, CD77, LIF and CCL12 (Fig. 1E and F). Furthermore, ten genes were differentially expressed in both the RNA sequencing and microarray datasets, namely: CCL13, CXCL2, MARCO, IL1R2, CXCR2, SELL, TREM1, C4A, C4B and S100A8 (Fig. 1G).

These gene expression changes highlight the complex immune and inflammatory responses induced by TBI, particularly impacting microglial cells. The upregulation of activating receptors such as TREM1, MARCO, IL1R2 and CXCR2 suggests activation and recruitment of microglia, monocytes and macrophages, essential for clearing damaged tissue and initiating repair. The increased expression of adhesion molecules and chemokines such as SELL, CXCL2 and CCL13 suggests the migration of immune cells to the injured brain tissue. C4A and C4B RNA expression are associated with complement system activation, which contributes to tissue clearance and infection defense. Likewise, the RNA expression of S100A8, by stimulating Toll-like receptors on microglial cells, serves a role in mediating inflammatory signal transduction.

Enrichment analysis. Metascape enrichment analysis demonstrated the most significantly associated pathways with the differentially expressed gene set from the previous analyses were: 'inflammatory response' (GO: 0006954); 'cytokine signaling in immune system' (R-HSA-1280215); 'Cytokine-cytokine receptor interaction' (hsa04060) and 'positive regulation of cytokine production' (GO: 0001819) (Fig. 2A). These findings show that many immune response pathways are activated after a TBI. They also show how important cytokine-mediated intercellular communication is for inflammation.

An enriched-term network was constructed to more effectively visualize the connections between each signaling pathway. Key nodes such as 'positive regulation of response to external stimulus' and 'positive regulation of leukocyte activation' were identified as crucial due to their central roles in the network. This highlighted their significance in regulating biological processes and disease states, especially in immune response and activation. Through this network analysis, researchers can better understand complex biological mechanisms and identify potential intervention points. Notable were the enrichments related to the NF-κB signaling pathway and neutral degranulation (Fig. 2B), because they are key to understanding how cells respond to external stimuli and regulate immune responses. Network nodes were color-coded by P-values in a further visualization, which demonstrated the statistically significant difference of most terms (Fig. 2C).

PPI enrichment analysis was performed to evaluate the interactions among differentially expressed genes at the protein level. Using the MCODE algorithm, the PPI network nodes were divided into ten modules, ranked by importance. This ranking was determined by considering various factors such as the density of connections among genes within a module, the size of the module, and its overall connectivity to key differentially expressed genes identified in the present study. For example, Module 1 involved signaling by interleukins, and Module 2 included cytokine-cytokine receptor interaction (Fig. 2D and E).

These analyses indicated that the inflammatory response predominated after brain injury. This involves varied intercellular signaling within the micro-environment of the nervous system, immune cell accumulation and activation of inflammatory pathways such as NF-κB.

Immune infiltration score. CIBERSORT analysis indicated significant increases in the number of macrophages M1 and M2, plasma cells and resting mast cells in the TBI group compared with the Sham group. Conversely, Treg cell, CD8 T cell, monocyte, follicular helper T cell, activated dendritic cell, activated mast cell and neutrophil levels were significantly decreased compared with the sham group (Fig. 3A). Furthermore, the cortex and hippocampus showed relatively higher macrophage proportions compared with the Sham

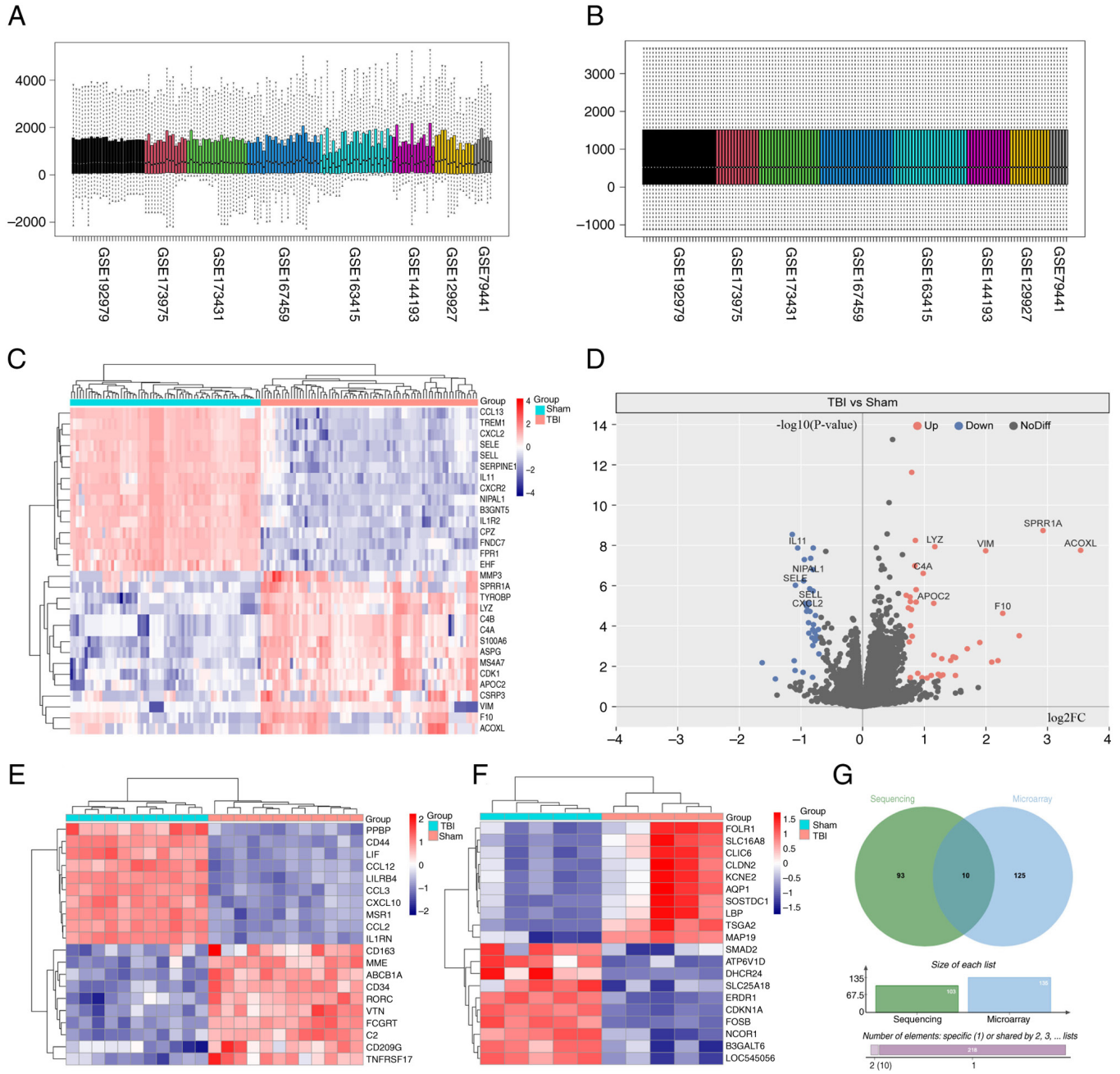

Figure 1. Microarray and high-throughput sequencing data processing and gene expression difference analysis. (A) Box plots of RNA expression before eliminating inter-sample differences and (B) after equalizing differences among samples, with each box representing a sample and different colors distinguishing datasets from various sources. (C) Heat map illustrating differential gene expression in the sequencing dataset, focusing on genes with the most significant differences between the TBI and Sham groups. (D) A volcano plot visualization of gene expression in the sequencing dataset. Heat map of differential gene expression in (E) Microarray dataset 1 and (F) microarray dataset 2. (G) Venn diagram depicting differentially expressed genes, with the green section representing sequencing gene sets and the light blue representing microarray gene sets.

group, and activated mast cells had a higher relative percentage in the hypothalamus than the Sham group (Fig. 3B).

The ESTIMATE method assessed overall immune infiltration, demonstrating significantly higher scores in the TBI group across all three metrics (ESTIMATE, immune score and stromal score) compared with the Sham group (Fig. 3C).

Immune infiltration increased slightly within one week following injury and declined over one month (no significant difference compared with the sham group; P>0.05). However, it gradually increased again during the chronic phase (2-3 months; significantly different compared with the sham group; P<0.05; Fig. 3D). The hippocampus exhibited the highest immune score, followed by the cerebral cortex (significantly different compared with the sham group; P<0.05). The thalamus and hypothalamus showed lower scores, with no significant differences between the TBI and Sham groups in these regions (Fig. 3E).

In summary, the immune and inflammatory responses following TBI are complex and multifaceted. Increases in macrophage levels, including the M1 and M2 sub-types, decreases in regulatory T cells and follicular helper T cells, and the enrichment of mast cells in specific brain regions indicate a

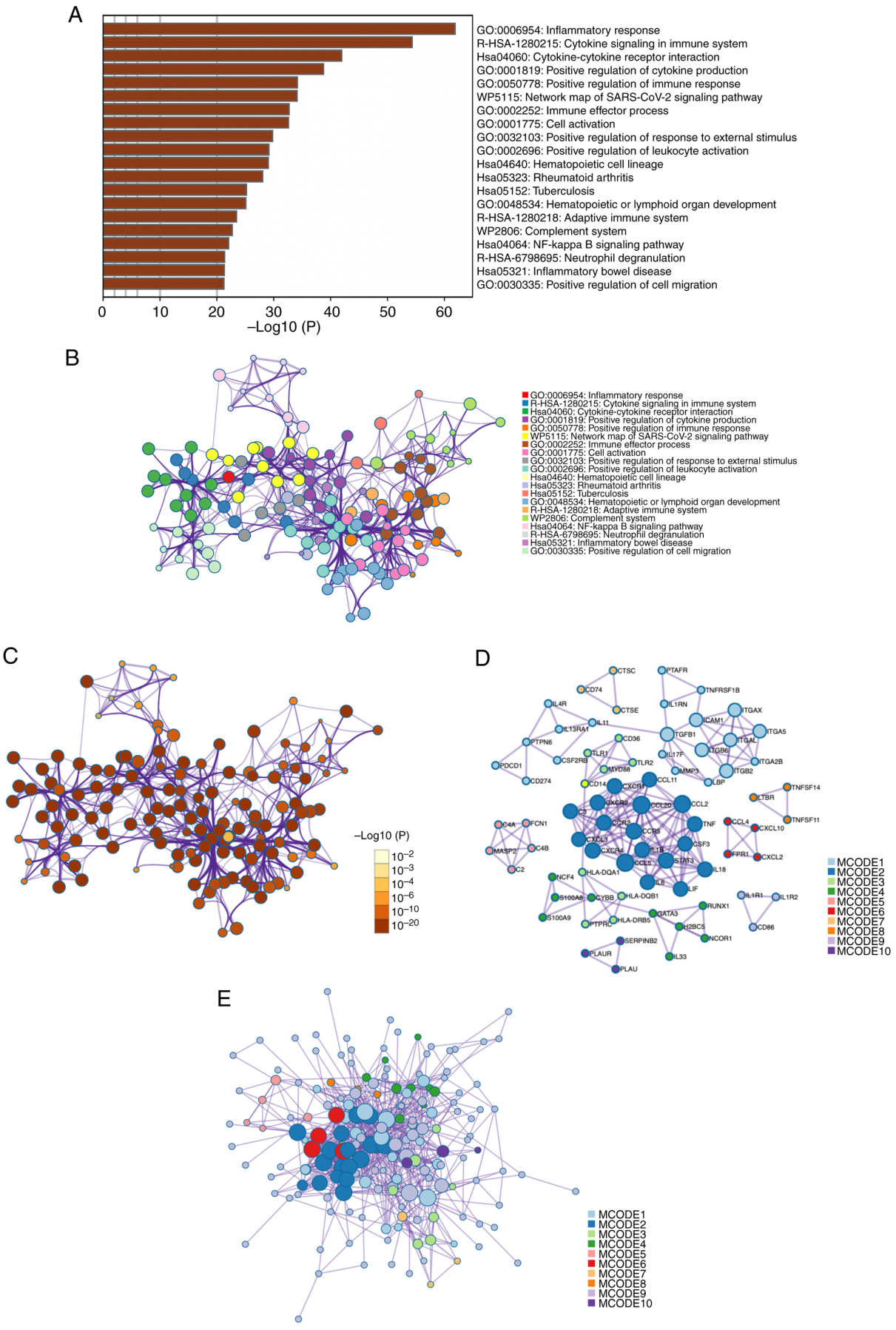

Figure 2. Enrichment analysis. (A) Bar graph of enriched terms across differentially expressed genes, displaying the top 20 clusters with representative terms. (B) Network of enriched terms, with nodes colored by cluster ID, grouping nodes with the same cluster ID. (C) Network of enriched terms, colored by P-value. (D) Protein-protein interaction network, employing the MCODE algorithm to identify densely connected network components. (E) Pathway and process enrichment analyses were conducted independently for each MCODE component. MCODE, Molecular Complex Detection.

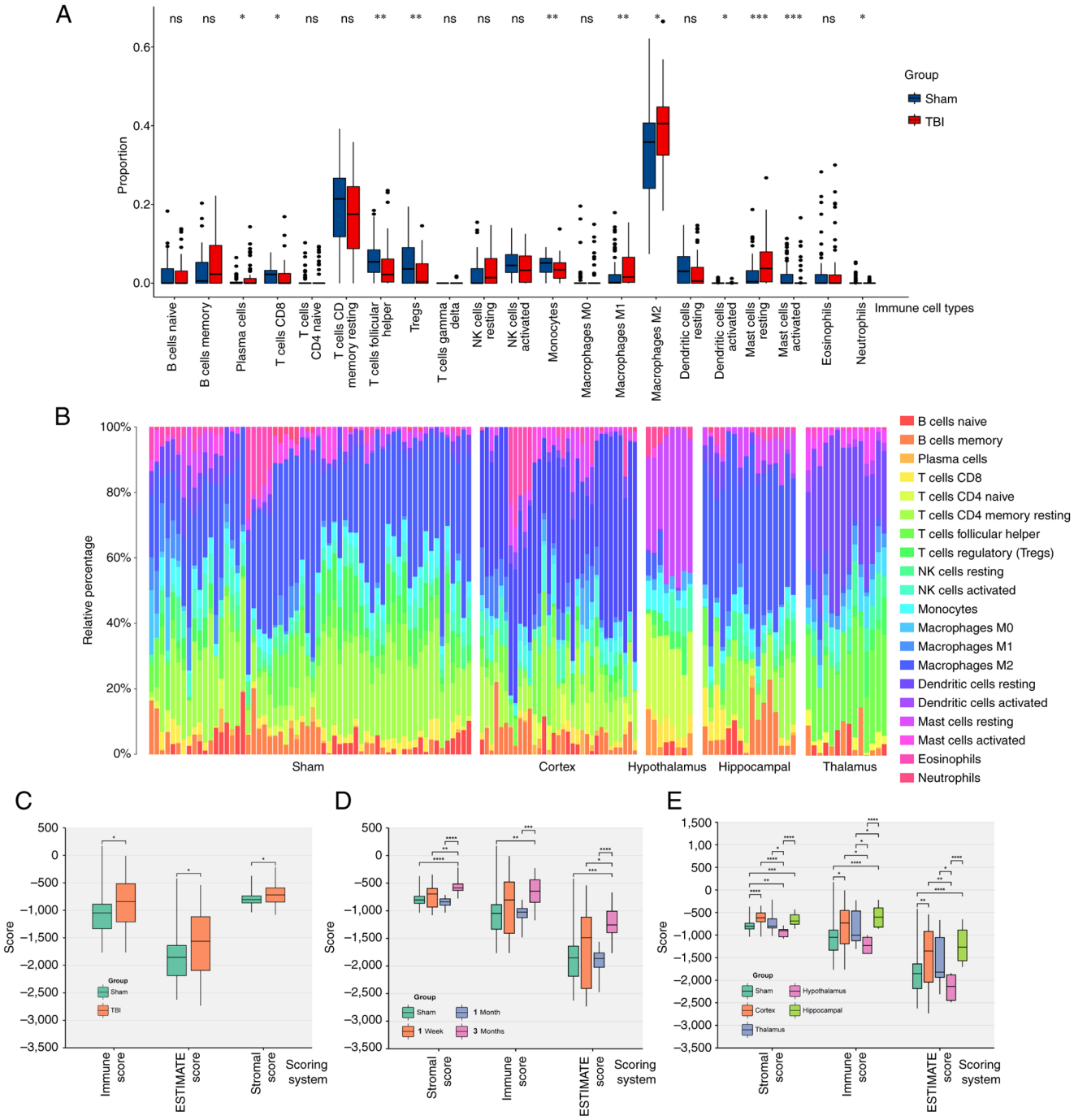

Figure 3. Immune cell infiltration score. (A) Comparison of the proportions of various immune cells infiltrating the brain between the Sham group and the TBI group. (B) Comparison of the proportions of immune cell infiltration in different brain regions between the Sham group and the TBI group. The rainbow chart reflects the proportions of various immune cells within brain tissue, where each color bar represents a brain tissue sample. (C) Comparison of the inflammation levels in brain tissue between the TBI group and the Sham group through three different scoring methods. (D) Comparison of the levels of inflammation at different time periods after brain injury. (E) Comparison of the inflammation levels in different parts of the brain after brain injury. *P<0.05, **P<0.01, ***P<0.001, ****P<0.0001. NK, natural killer; ns, non-significant; TBI, traumatic brain injury.

dysregulation of the immune system and an amplified inflammatory response, especially during the chronic phase (3 months after the brain injury) after TBI. These dynamic changes in immune cell profiles and variations in immune scores across different brain regions highlight the need for personalized and targeted inflammation modulation in TBI treatment.

WGCNA. The data from the RNA sequencing datasets processing revealed no missing values or outliers within the datasets. Following the construction of an automatic network and module detection, a soft threshold of 15 was recommended. In this network, nodes represent genes, and edges represent co-expression relationships between genes. Modules are clusters of genes closely related within the network. The soft threshold plays a role in filtering co-expression relationships in gene co-expression network analysis, aiding in determining the strength of network connections, thus influencing the results of module detection. The curve begins to flatten at

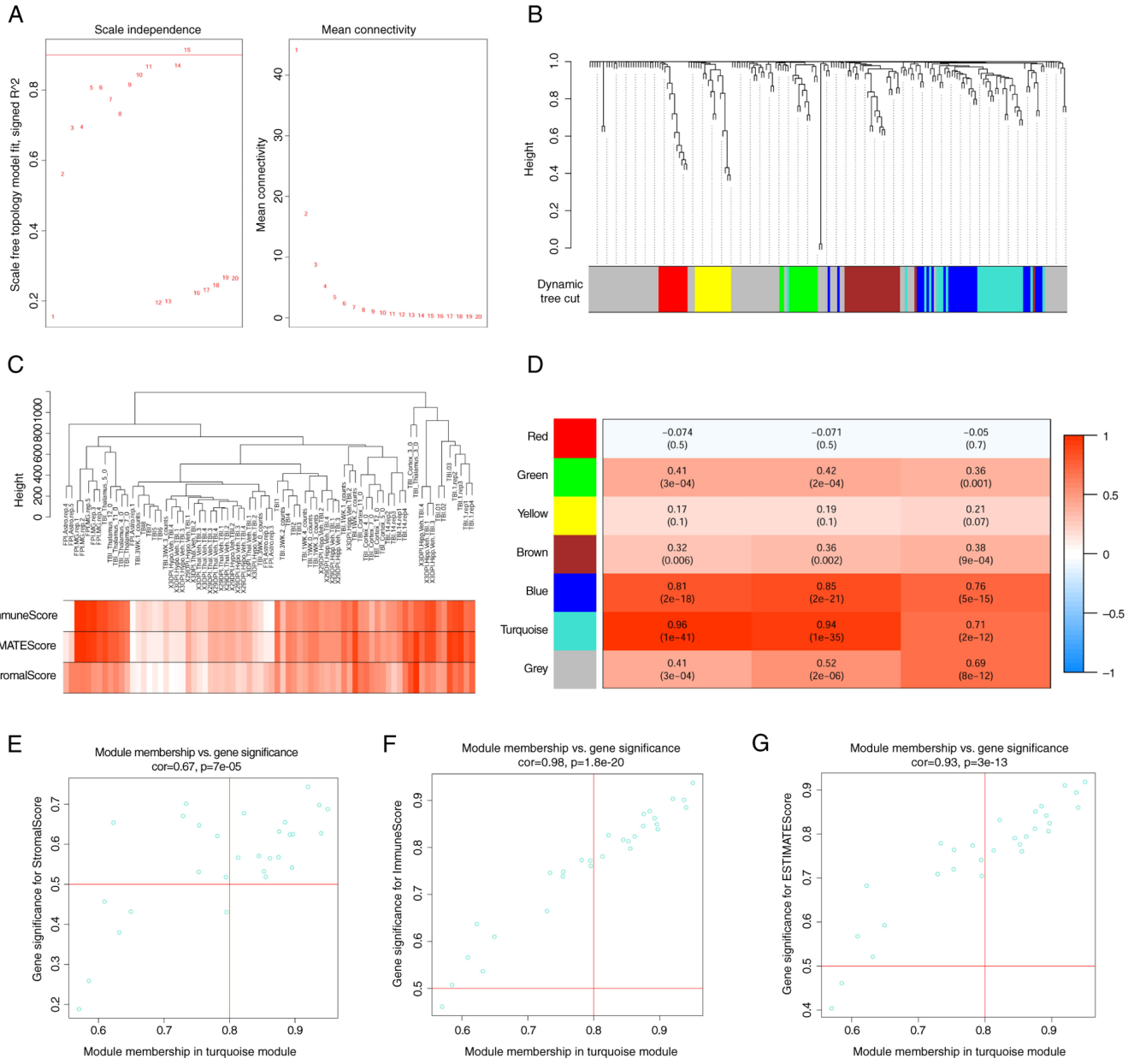

Figure 4. Weighted gene co-expression network analysis. (A) The recommended soft threshold is indicated above the red line (left) and trend of mean connectivity (right). (B) Gene dendrogram and module colors, with each branch representing a gene and each color block a co-expression gene set. (C) Sample dendrogram and trait heatmap, where heatmap color depth represents the correlation between genes and phenotypes. (D) Module-trait relationships heatmap, with color depth indicating the correlation degree between module genes and immune cell infiltration. Scatter diagram of module membership. The numbers within the squares represent the correlation coefficients and P-values for samples within each group. (E) vs. gene significance for StromalScore, (F) ImmuneScore and (G) ESTIMATE.

this threshold, suggesting satisfactory average connectivity (Fig. 4A). Using the 'blockwiseModules' function, 228 differentially expressed genes were classified after TBI into seven co-expression modules. A hierarchical clustering tree diagram was generated for module identification (Fig. 4B).

Module-phenotype data analysis indicated that the turquoise module had the highest correlation with the immune score (Fig. 4C and D). This module contained 29 co-expressed genes, including LYZ, TYROBP, CDK1, PDCD1 and RGS1. From this a gene significance-module membership, a scatter plot for these genes was created. This plot illustrated two main points: First, it showed how closely related the genes within the turquoise module were to each other, referred to as their module membership. Second, it highlighted the association between the importance of each gene to the immune response (gene significance) and their affiliation with the turquoise module (Fig. 4E-G).

The immune-related module gene set from WGCNA analysis was entered into the STRING database for PPI network analysis. This confirmed the relevance of these genes and their key roles in the immune response. Screening for key node genes with >4 connections identified seven critical nodes: TYROBP, CCR5, PTPRC, ITGB2, FCGR2B, TLR2 and CD86 (Fig. 5A).

Cell death. Current scientific understanding indicates that brain injury leads to neuronal death through numerous

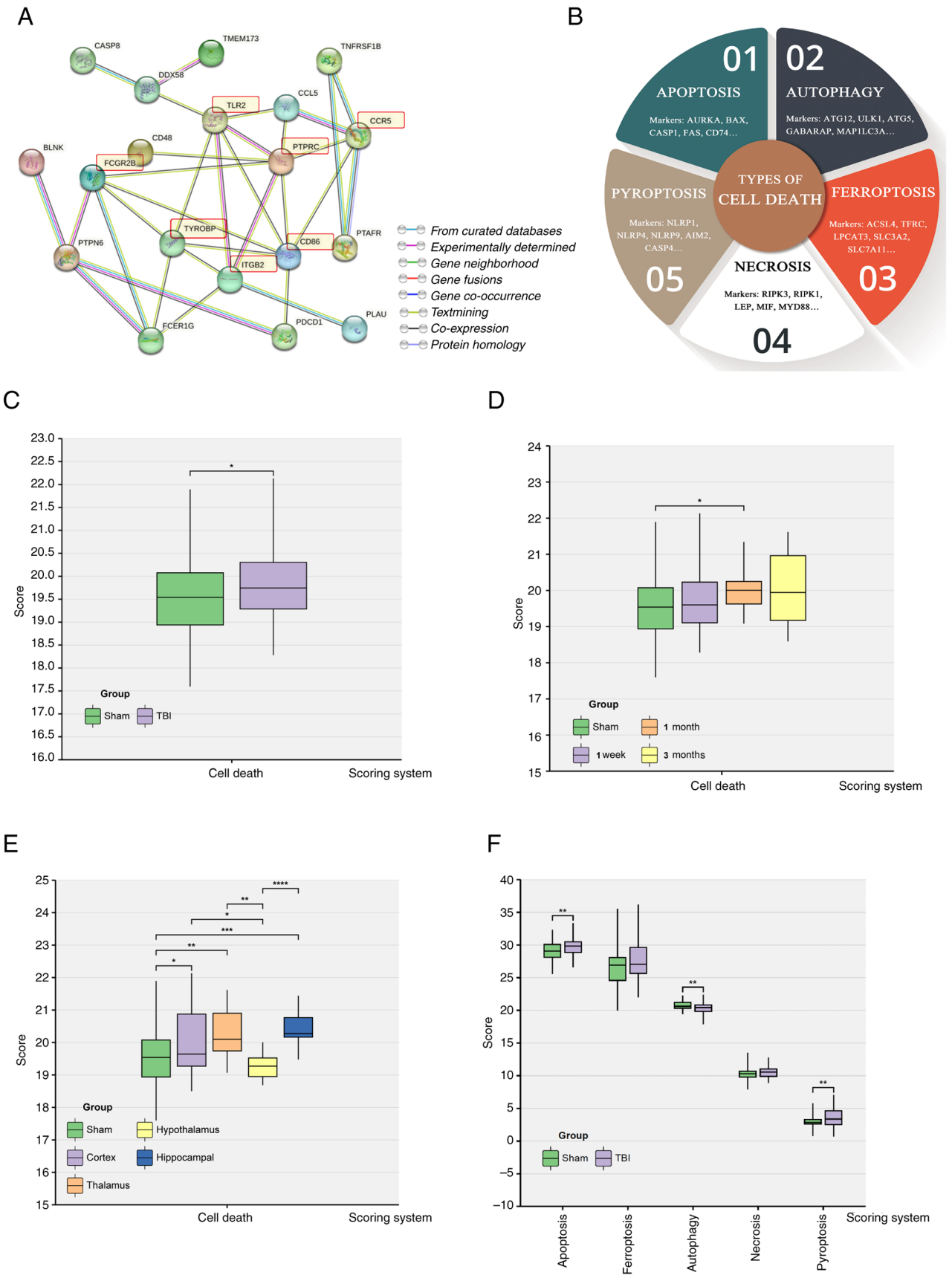

Figure 5. Cell death score. (A) A STRING network constructed using immune-related co-expression gene sets identified by WGCNA, where each node represents proteins produced by a single gene locus. Edges represent protein-protein associations, with key nodes marked in red boxes. (B) Construction of cell death scores through recognized data sets, displaying parts of marked genes. (C) Comparison of brain cell death scores between the Sham and TBI groups. (D) Comparison of cell death scores at different times in the TBI and Sham groups. (E) Comparison of cell death scores among different tissues in the TBI and Sham groups. (F) Comparison of five cell death scores between the Sham and TBI groups. *P<0.05, **P<0.01, ***P<0.001, ****P<0.0001. TBI, traumatic brain injury; STRING, Search Tool for the Retrieval of Interacting Genes/Proteins; WGCNA; weighted gene co-expression network analysis; MCODE, Molecular Complex Detection.

pathways. The present study assessed the five most prominent cell death modalities; apoptosis, necrosis, autophagy, ferroptosis and pyroptosis (Fig. 5B).

Results showed that the overall cell death index in the TBI group was significantly higher compared with that in the Sham group (Fig. 5C). In TBI, brain cell mortality in mice was significantly increased at one month compared with the Sham group (Fig. 5D). The cerebral cortex, hippocampus, and thalamus exhibited significantly higher cell death indices compared with the Sham group. In contrast the hypothalamus had a markedly lower cell death index compared with the Sham group (Fig. 5E). Furthermore, there were higher levels of apoptosis and pyroptosis than other forms of brain cell death after trauma. The autophagy score was significantly lower in the TBI group compared with the Sham group (Fig. 5F).

These results indicated that most cell death occurred within one month after trauma, highlighting a crucial period for therapeutic intervention. Apoptosis and pyroptosis were demonstrated as the predominant cell death mechanisms after brain trauma and present potential targets for treatment. Likewise, increasing the levels of autophagy may increase neuronal resilience against injury, starvation and oxidative stress, making it a potential intervention strategy.

Cluster analysis. Using the 'ConsensusClusterPlus' method, a consistency matrix for different grouping numbers (K) was constructed. The analysis showed stable cluster assignments at K=2, with new clusters becoming small and less reliable at K>2 (Fig. 6A). Empirical cumulative distribution plots indicated stable data results for K between 2 and 4 (Fig. 6B and C).

After grouping, gene expression was depicted in a heatmap, which indicated significantly higher expression of immune key node genes in group 1 compared with group 2 (Fig. 6D).

When comparing cell death scores, group 1 exhibited significantly higher ferroptosis, necrosis and pyroptosis scores, and a significantly lower autophagy score compared with group 2 (Fig. 6E). This suggested that immune-related node genes in TBI were linked to ferroptosis, necrosis and pyroptosis in the nervous system after brain trauma and were inversely associated with autophagy.

These insights reveal unique pathological characteristics of TBI, emphasizing the role of various cell death pathways in exacerbating neuronal damage and impairing neural functions. Targeted approaches, such as regulating iron metabolism, using antioxidant treatments or inhibiting inflammatory death pathways, combined with enhancing autophagy, could be effective strategies for reducing neuronal injury and aiding nervous system recovery.

Single-cell sequencing analysis. Three single-cell sequencing datasets were integrated related to TBI, and quality control was performed to ensure data accuracy. To mitigate batch effects, the Harmony method was used (Fig. 7D), yielding 37,621 high-quality cells. Using the tSNE method, the sequencing samples were classified into 12 cell types based on specific marker genes (Fig. 7A). Notably, in the TBI group, there was an increase in the proportion of microglia and macrophages (Fig. 7B), suggesting their role in the inflammatory process in TBI. The annotation method and markers for cell types have been organized (Fig. 7C).

Pseudotime analysis demonstrated that after TBI, microglia underwent three evolutionary nodes and differentiated into two distinct paths. This suggests TBI causes microglia to diverge into two functional states, highlighting their complex response to injury. Using these nodes, 'monocle2' further categorized the microglia into 7 clusters (Fig. 7E). These findings indicated that, after TBI, microglia diverge into two paths: Cluster 6, which promoted chronic inflammation and cell death via cell fusion, and Cluster 7 which reduced inflammation by downregulating interleukin 6 (Fig. 7F). The former may lead to sustained neuronal tissue damage, whereas the latter could help attenuate inflammation and preserve neural cells, providing crucial treatment insights. TYROBP is key in controlling microglia differentiation and activity, essential for improving TBI prognosis and neural recovery. The present analysis analysis showed TYROBP consistently highly expressed over time, emphasizing its crucial role in cell differentiation and microglial modulation. This suggested that s targeting TYROBP could significantly aid TBI recovery. (Fig. 7G). Hence, targeting the TYROBP pathway to regulate these mechanisms offers a potential target for TBI therapeutic strategies.

The distribution of previously identified immune-related key node genes including CD86, CCR5, PTPRC, TLR2, FCGR2B, ITGB2, TCGR2B and TYROBP in TBI was also analyzed. The results showed that these genes were mainly found in microglia, macrophage and monocyte nuclear dendritic cells (Fig. S1A and B). This suggested the activation of various immune cells after brain trauma, with innate immune cells serving a role in nervous system inflammation after injury.

Using the 'SCENIC' package in the R, transcription factor activity across different cell types in TBI single-cell sequencing data was analyzed. It is suggested that RUNX1 might act as an upstream transcription factor for genes like TYROBP, influencing microglial cell activation and response, potentially linking to neurodegenerative diseases and neuroinflammation following brain injury (Fig. S2 and 3).

Cell-cell communication analysis. Cell-cell communication analysis is used to assess paracrine and autocrine signaling, particularly under pathological conditions that alter the tissue micro-environment. The present study demonstrated enhanced signaling pathways of CCL, CX3C, PTN, PSAP, GALECTIN, MK and EDN in the TBI group compared with the Sham group. Conversely, the intercellular communication pathways TGF-β, VEGF, CXCL, GAS, PDGF and TNF were decreased (Fig. 8A and B). These dynamics, detailed in Fig. 8A and B, suggested a balance between recovery promotion and excessive inflammation prevention, crucial for TBI treatment strategies.

Notably, the interaction between CCL5 and CCR5 intensified after brain injury (Fig. 8C), potentially influencing the accumulation of microglia and macrophages in the affected area. Overall, there was increased communication among neurons, astrocytes, microglia and neighboring cells following injury (Fig. 8D). Furthermore, microglia and macrophages, the primary innate immune cells in the central nervous system, were further assessed. It was demonstrated that after injury, microglia receive paracrine signals from

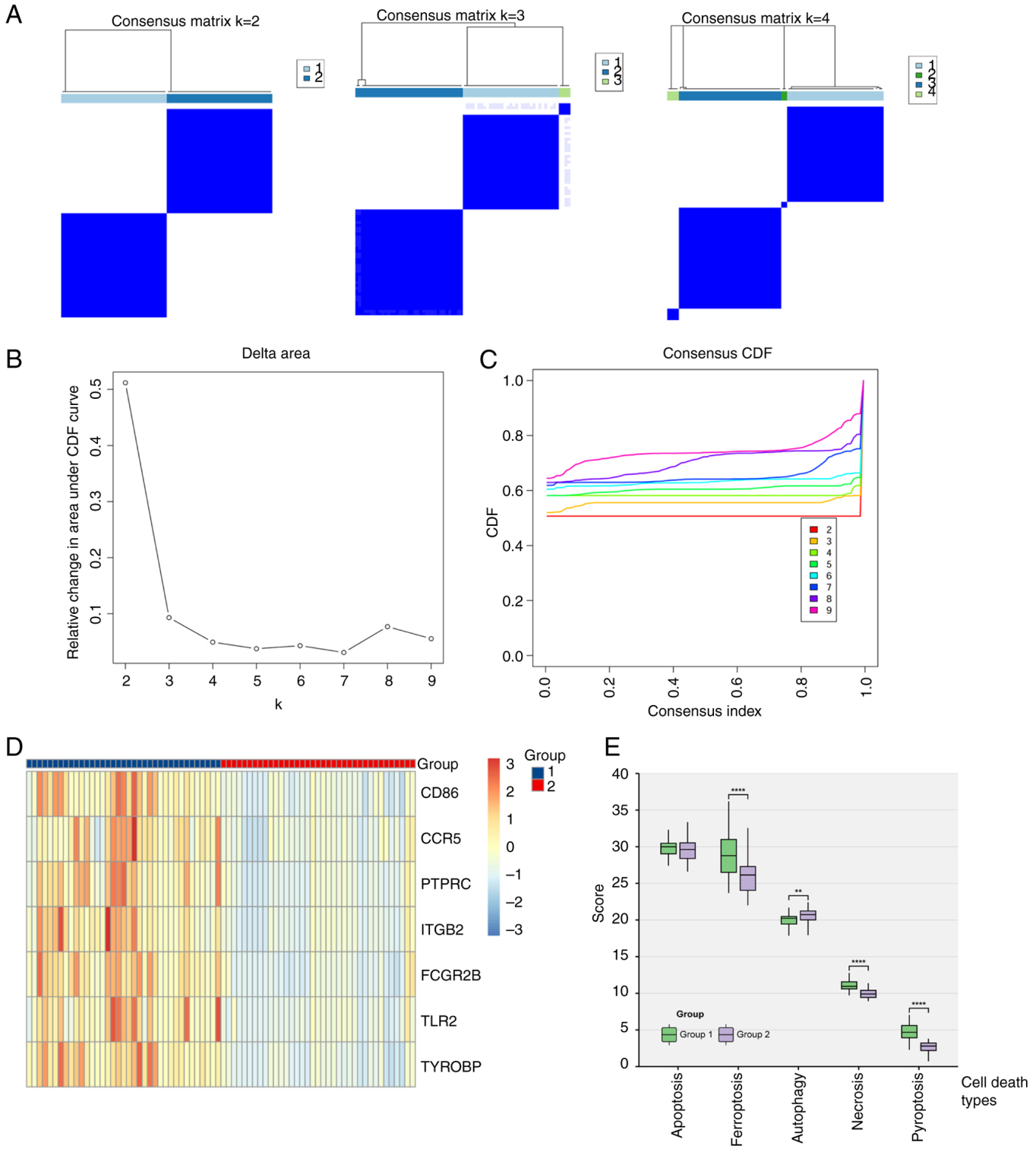

Figure 6. Cluster analysis. (A) Consensus matrix for each k (number of clusters), showing consensus values on a white-to-blue color scale, ordered by consensus clustering, shown as a dendrogram, with consensus clusters marked by colored rectangles. (B) Delta area plot displaying relative change in area under the CDF curve for each k. (C) CDF plot displaying consensus distributions for each k. (D) Heat map of gene expression by group, based on cluster analysis results. (E) The differences in five cell death modes among groups. **P<0.01, ****P<0.0001. CDF, Empirical cumulative distribution function.

various cell types, including neurons, astrocytes, endothelial cells and other immune cells (Fig. 8E). These signals potentially prompt migration to the damaged sites for cell repair and regeneration.

Hierarchical analysis indicated a reduction in intercellular communication signals received by oligodendrocyte precursor cells after injury, including factors for cell growth and differentiation including TGF-β, VEGF and PDGF (Fig. 8F). This could hinder oligodendrocyte maturation, leading to neural repair disorders and demyelinating diseases. Moreover, the role of the CCL pathway in recruiting and phagocytosis of innate immune cells was also demonstrated. The evidence leading to

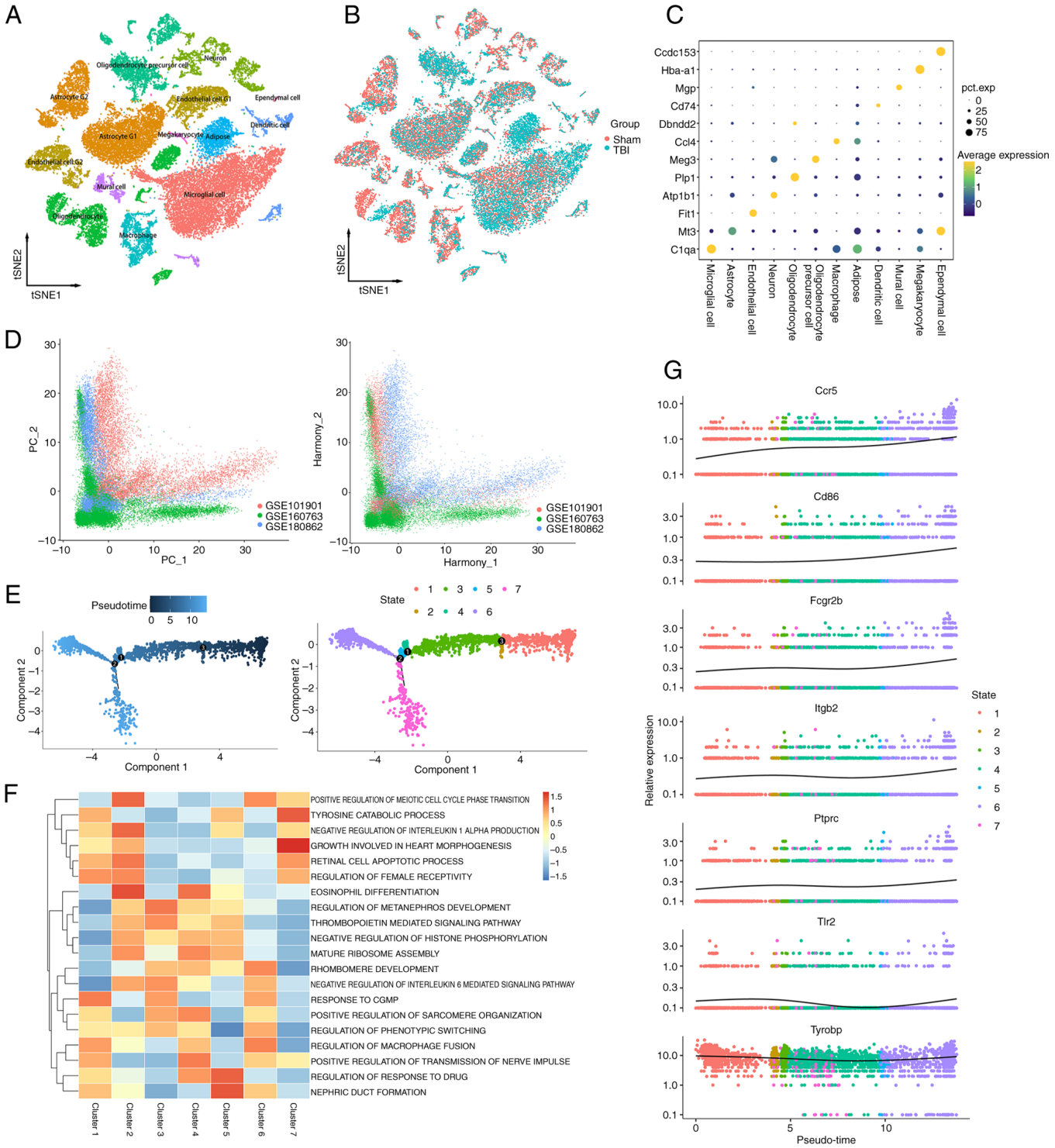

Figure 7. Single-cell dataset collation and annotation (A) Post-merger tSNE method for dimension reduction in single-cell sequencing datasets, with cells in Sham and TBI groups labeled. (B) Annotation of 12 cell types in the combined single-cell sequencing dataset. (C) Dot plot displaying marker genes of annotated cells. (D) Batch effect between samples from different sources (left) and reduction in group differences post-Harmony method batch effect removal (right). (E) Microglia pseudotime analysis results, with coloring by pseudotime (left) and cell clusters divided by time nodes (right). The numbers within the black circles represent nodes of cell differentiation. (F) GSVA enrichment analysis, with rows representing biological processes of cell clusters and columns representing pseudotime cell clusters. (G) Gene expression is ordered by pseudotime, with black lines indicating gene expression trends and dots representing cells on the pseudotime trajectory. tSNE, t-distributed stochastic neighbor embedding; TBI, traumatic brain injury; GVSA, gene set variation analysis; pct. exp; percentage expression.

this conclusion was derived from a series of analyses focused on the TBI group, specifically looking at the interactions mediated by the CCL pathway (Fig. 8G and H), which suggested that a balance between microglia and oligodendrocytes is important for immune system homeostasis during inflammation caused by TBI.

The clustering analysis of cell communication identified a specific signal pattern (Pattern 1) associated with microglia,

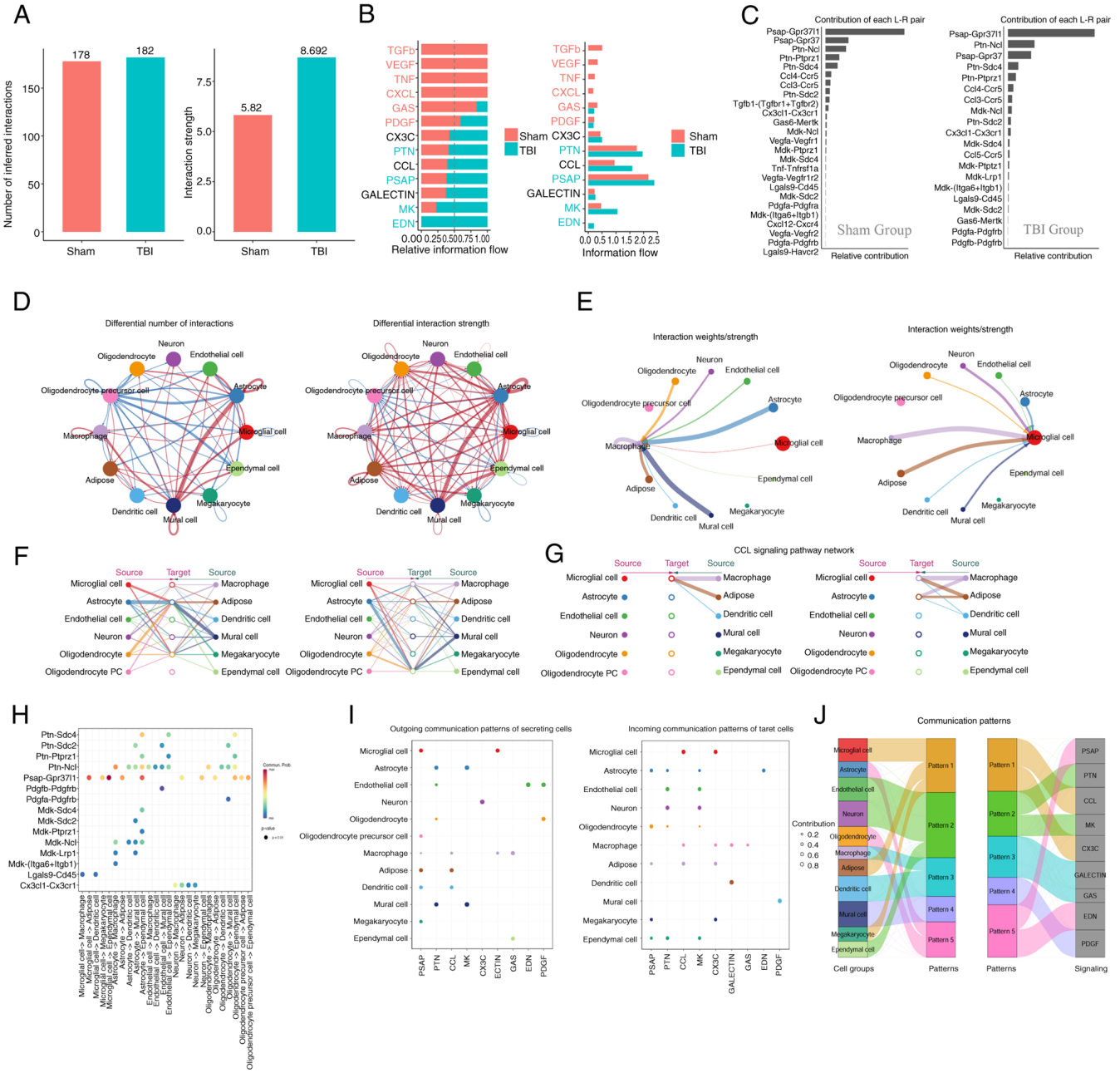

Figure 8. Cell-cell communication analysis. (A) Number of inferred interactions between Sham and TBI groups (left) and interaction strength (right). (B) Relative information flow between the Sham and TBI groups (left) and Information flow (right). (C) Contribution of each ligand-receptor pair in the Sham group (left) and TBI group (right). (D) Circle plot of intercellular communication, showing differential interactions between Sham and TBI groups (left) and differential interaction strength (right). The red line indicates enhanced cell communication after brain injury, while the blue line indicates weakened cell communication after brain injury. (E) Communication signals transmitted to microglia from other brain cells (left) and signals transmitted to macrophages (right). Hierarchical diagram of (F) Intercellular interaction and (G) The CCL signaling pathway in the TBI group, with signal sources on the left and right and signal targets in the middle. (H) Diagram of ligand-receptor pair transmission signal direction in the TBI group. (I) Communication patterns of secreting cells in the TBI group. (J) Inferred communication patterns of target cells in the TBI group illustrate the correspondence between latent patterns, cell groups and signaling pathways. Connection thickness indicates the contribution of each cell group or signaling pathway. TBI, traumatic brain injury.

involving the release of the chemokines CCL and CX3C at the injury site and immune cell activation via the TNF or TGF-β pathways (Fig. 8I). The TNF pathway, induces programmed cell death in inflammatory states, and TGF-β regulates cell growth, differentiation and apoptosis. These results indicate the dual role of microglia in immune regulation, mediating both cell repair and death. Additionally, the present analysis of macrophage-related cell communication patterns demonstrated their associated pathways including CCL, TNF, GSA and GALECTIN (Fig. 8J). These patterns illustrated how different cell types respond to specific signaling cues within their microenvironment. The GSA pathway, involving NF-κB, TNF and MAPK, serves a role in reducing inflammation and apoptosis. Likewise, GALECTIN is an important part of innate immunity and is recognized by danger-associated molecular patterns. It controls the activity of macrophages and microglia and could be used as a treatment target for neurodegenerative diseases.

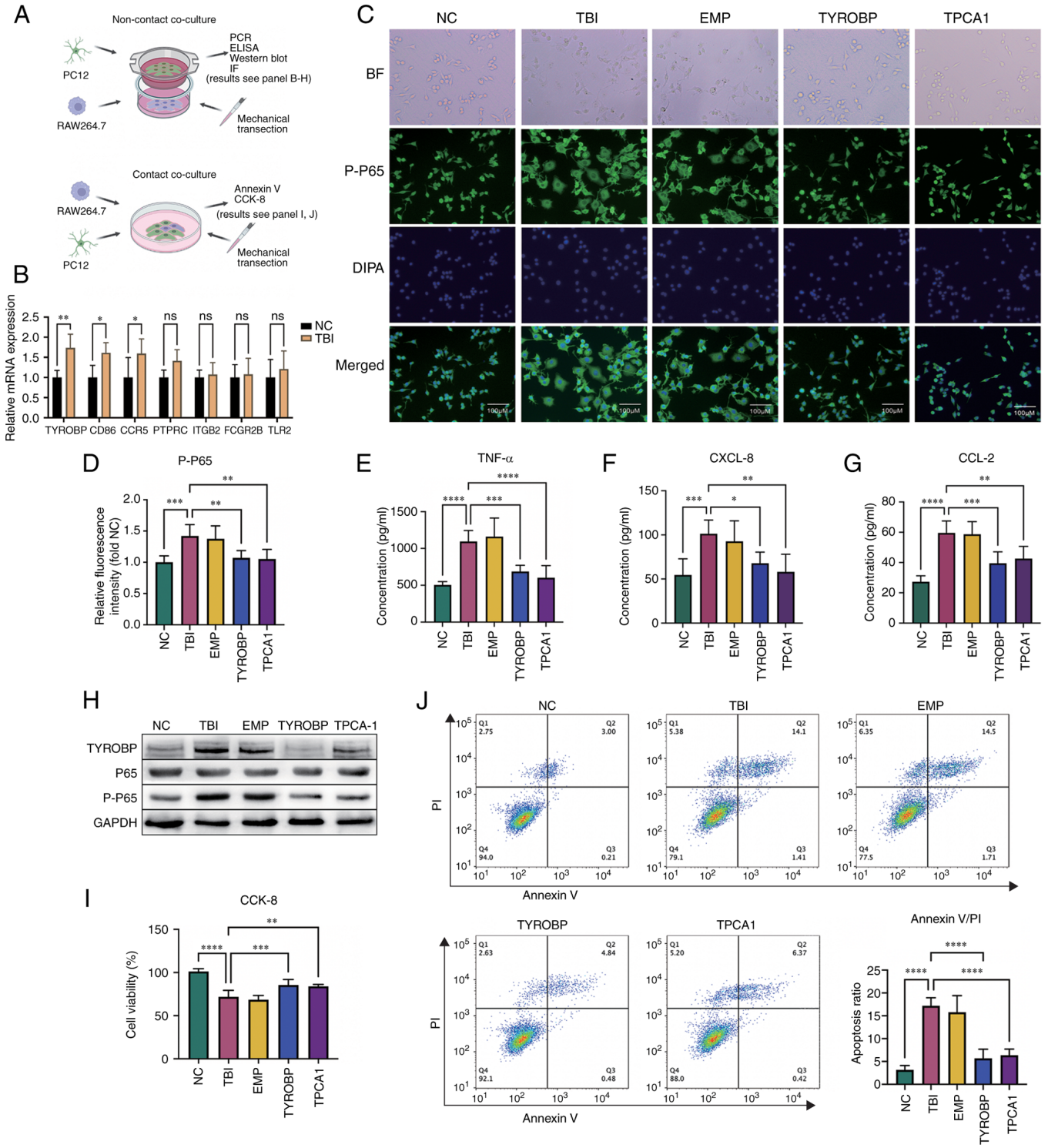

Figure 9. Impact of TYROBP on microglial activation. (A) Schematic of the experimental procedure showing the non-contact co-culture model of RAW264.7 and PC12 cells to study microglial activation after TBI (above) and a contact co-culture model to investigate neuronal apoptosis (below). (B) Reverse transcription quantitative polymerase chain reaction assessing the relative mRNA expression levels of surface antibodies in RAW264.7 cells in the TBI and Sham groups. (C) Immunofluorescence experiments depicting the levels and distribution of P-P65 in RAW264.7 cells. (D) Comparison of the average fluorescence intensity of P-P65 in immunofluorescence experiments. Enzyme-linked immunosorbent assay (ELISA) measuring cytokine expression levels of (E) TNF-α, (F) CXCL-8 and (G) CCL2 in the PC12 and RAW264.7 cell co-culture systems, with paired comparisons to the TBI group. (H) Western blotting detected TYROBP expression and NF-κB pathway activation status via P65 phosphorylation under varying conditions. (I) CCK-8 assays comparing cell viability in each group, with the average OD of the NC group as 100% survival for reference calculated as, cell viability=(OD_{sample}-OD_{blank})/($OD_{control}$-OD_{blank}). (J) Annexin V-PI assay determining cell apoptosis proportions, with the bar chart in the lower right corner summarizing the proportions of early-stage (annexin V positive, PI negative) and late-stage apoptotic cells (both annexin V and PI positive). *P<0.05, **P<0.01, ***P<0.001, ****P<0.0001. TBI, traumatic brain injury; P-P65, phosphorylated P65; PI, Propidium iodide.

Neuron-microglia interaction experiment. To model TBI *in vitro*, we employed two distinct co-culture systems were employed: A non-contact co-culture system, designed to evaluate the impact of brain injury on microglial cell

activation; and a contact co-culture system, aimed at assessing neuronal cell survival following brain injury (Fig. 9A). Using RT-qPCR, the mRNA expression levels of seven receptor types in RAW264.7 cells, which act as microglia-like models were measured. Statistically significant differences in three receptors were found between the NC and TBI model groups (Fig. 9B). Notably, the levels of TYROBP in the TBI model were significantly increased 1.8-fold compared with the control (Fig. 9B). Consequently, the role of TYROBP in TBI was further assessed.

In the immunofluorescence experiment, RAW264.7 cells co-cultured with injured PC12 cells demonstrated marked morphological changes, including a larger cell volume and increased pseudopodia formation, indicative of an inflammatory response. However, RAW264.7 cells with TYROBP gene knockouts did not exhibit these changes, which suggested the involvement of TYROBP in this response. Cells in the TPCA1 treatment group also lacked these morphological changes observed in the TBI group, while the empty plasmid group showed no inhibition of these changes, confirming that the plasmid itself did not affect cell morphology (Fig. 9C).

The relative intensity of fluorescence signal of phosphorylated P65 were significantly increased in the TBI group compared with the NC group, which indicated NF-κB pathway activation in the inflammatory response. However, in TYROBP knockout RAW264.7 cells, the phosphorylated P65 signal was significantly decreased compared with the TBI group, which suggested a regulatory effect of TYROBP in P65 phosphorylation. Likewise, the TPCA1 treatment group had a significantly decreased signal compared with the TBI group, whereas the empty plasmid group did not, further confirming the non-inhibitory effect of the empty plasmid on P65 phosphorylation (Fig. 9D). These results reinforce the potential role of TYROBP in the inflammatory response.

In ELISA experiments, cytokine levels were measured in the co-culture medium. TNF-α (Fig. 9E), CXCL4 (Fig. 9F) and CCL2 (Fig. 9G) cytokine levels were low in the NC group. However, their levels significantly increased in the TBI group compared with the control, which suggested the successful induction of the inflammatory TBI model. In the empty plasmid group, TNF-α, CXCL4 and CCL2 levels remained high, which demonstrated that the empty plasmid did not significantly affect cytokine expression. In the TYROBP treatment group, the levels of TNF-α, CXCL4 and CCL2 were significantly decreased compared with the TBI group, suggesting a potential anti-inflammatory effect of TYROBP. Likewise, TPCA1 also significantly reduced the levels of TNF-α, CXCL4 and CCL2 compared with the TBI group. These results suggest the potential of TYROBP as an anti-inflammatory target, acting through TNF-α, CXCL8 and CCL2 signaling pathways.

Western blotting showed that the TBI group had markedly higher levels of TYROBP protein expression compared with the NC group and this was decreased in the TYROBP knock out group. The P65 protein levels remained consistent between the groups, but the level of phosphorylated P65 was increased in the TBI group compared with the control and decreased in the TYROBP group compared with the TBI group, which suggested that TYROBP serves a role in the phosphorylation of P65. Likewise, TPCA1 also decreased the levels of P65 phosphorylation compared with the TBI group, and the empty plasmid levels were consistent with the TBI group, showing no notable effect on protein expression. GAPDH, the housekeeping protein, displayed consistent levels across all groups, which confirmed the western blotting reliability (Fig. 9H).

To further assess the impact of activated microglia on neuronal apoptosis following TBI, a CCK-8 assay was performed to count surviving PC12 cells 24 h after brain injury. The results demonstrated a significant decrease in cell viability in the TBI group compared with the control, thereby validating the TBI model. In the TYROBP group, there was a significant increase in cell viability in the TBI group compared with the TBI group, which indicated the possible role of TYROBP in neuronal survival. Furthermore, treatment with the IKK-2 inhibitor, TPCA1, also significantly increased PC12 cell viability compared with the TBI group, suggesting the cytotoxic effect of microglia was mediated by the NF-κB signaling pathway. Furthermore, the cell viability in the EMP group mirrored that of the TBI group, demonstrating that the empty plasmid did not affect the cell viability (Fig. 9I).

Annexin V/PI double staining, a common flow cytometry method was used to evaluate cell apoptosis and death. This technique distinguishes early apoptotic, late apoptotic, necrotic and viable cells by using annexin V and PI concurrently. These findings showed that cells in the NC group exhibited a small fraction of apoptotic cells (annexin V positive) and a very low proportion of necrotic cells (PI positive, annexin V negative), likely due to manipulation during cell culture. In the TBI group the number of necrotic cells increased significantly compared with the control, which confirmed the successful establishment of the TBI model. Likewise, the proportion of apoptotic cells in the TBI group significantly increased compared with the control. In the TYROBP group, the proportion of apoptotic cells significantly decreased compared with the TBI group, supporting the earlier observation that TYROBP gene knockout in Raw264.7 (microglia-like cells) had a neuroprotective effect. Cells in the TYROBP knockout group exhibited a lower proportion of necrotic cells. This reflected the protective role of TYROBP knockout in cellular damage responses by promoting neuronal survival, reducing apoptosis, enhancing repair and ultimately mitigating necrosis caused by scratch injuries. After PCA1 treatment, the proportion of apoptotic cells also significantly decreased compared with the TBI group, suggesting a detrimental impact of NF-κB pathway activation on neurons. The empty plasmid group showed no significant change compared with the TBI group, allowing the exclusion of confounding factors in the experiment (Fig. 9J). It should be noted that when selectively separating PC12 cells in a co-culture medium, a small amount of RAW264.7 cells may still be present. However, since the proportion of RAW264.7 cells is inherently low, this does not affect the experimental results.

Discussion

Neuroinflammation is a pathological feature of acute neurological dysfunction and chronic traumatic encephalopathy following TBI (28). Microglia, as the primary cells of the innate immune system in the central nervous system (CNS), serve a crucial role in neuroinflammation after TBI (29). During brain injury, microglia can produce neurotrophic

factors, clear cellular debris and orchestrate neural recovery processes, which are beneficial for recovery after TBI. However, microglia may also become dysregulated, potentially producing high levels of pro-inflammatory cytokines and cytotoxic mediators, thereby hindering CNS repair and leading to neuronal dysfunction and cell death. Their activation state and functional responses following TBI have been suggested to determine whether microglial activation is advantageous or detrimental to neurons (30).

In the present study, the mechanisms of microglial activation following TBI were assessed using microarray, mRNA sequencing and single-cell analysis. The activation state of microglia was assessed by observing changes in the morphology of microglia-like cells, activation of inflammation-related signaling pathways and cytokine expression. These results indicate that after TBI, there are alterations in the interaction networks among various cells in the nervous system. Particularly, interactions with neurons seem to be crucial in triggering microglial activation. Suggesting that modulation of these interactions could enhance neuronal vitality and reduce cell death rates.

Furthermore, seven key molecules that regulate the inflammatory process after TBI were identified. These include CD86, a member of the immunoglobulin super-family that stimulates T-cell activation and cytokine secretion (31); CCR5, a G protein-coupled receptor super-family member that regulates immune cell migration and proliferation (32); PTPRC, a transmembrane glycoprotein crucial for innate immunity, whose imbalance leads to immune disorders (33); ITGB2, an intercellular adhesion molecule receptor influencing natural killer (NK) cell cytotoxicity and supporting T-cell and neutrophil functions (34); FcγRIIB, a protein that modulates the innate immune system, inhibits Toll-like receptors, and impacts B cell and dendritic cell migration (35); and TLR2, a protein involved in innate immunity and associated with adaptive immunity, which recognizes pathogen structural molecules and triggers an immune response. Notably, TYROBP, a transmembrane adaptor protein and signaling partner for multiple immune-related receptors, is essential for maintaining the stability of the immune micro-environment of the brain (36).

TYROBP is predominantly expressed in certain myeloid cells and NK cells, and research indicates its primary expression in microglia within the CNS and peripheral macrophages (37). TYROBP has an immune receptor tyrosine activation motif (ITAM) in its cytoplasmic domain. TYROBP forms complexes with companion membrane receptors, though its extracellular domain is short and it cannot bind to ligands. Ligand binding to a TYROBP-associated receptor activates TYROBP through the ITAM in its cytoplasmic domain, triggering cellular activation responses such as cytokine production, cell proliferation and macrophage survival (38,39). Moreover, TYROBP serves a crucial role in osteoclast differentiation, antigen presentation and the maturation and survival of dendritic cells, underscoring its regulatory role in immune and cell activation processes (40).

The effect of TYROBP on the NF-κB signaling pathway remains a topic of debate. It has been proposed that TYROBP serves a role in immune responses by associating with certain immune receptors, such as KIR receptors on NK cells and TREM2 on myeloid cells (41). This association facilitates signal transduction within the cell, leading to TYROBP phosphorylation upon ligand recognition, activating downstream signaling pathways including PI3K/AKT and Syk, which are crucial for NF-κB activation, thereby triggering various immune responses (42). Another study has suggested that TYROBP activates Syk kinases, directly or indirectly triggering key molecules in the NF-κB pathway, such as the IKK complex (43). Additionally, TYROBP activation is considered to affect intracellular calcium ion flow, further activating NF-κB through calcium-dependent protein kinases like PKC (44). A theory also posits that TYROBP influences the expression of pro-inflammatory or anti-inflammatory cytokines by microglia, thereby affecting microglial activation through pathways other than NF-κB (45). Thus, the role of TYROBP in microglial activation and its interaction with the NF-κB signaling pathway remain an area of ongoing research.

The present study suggested that the TYROBP gene is involved in microglial activation after TBI. TYROBP activates the downstream NF-κB signaling pathway in response to exogenous stimuli or endogenous inflammatory factors. Once activated, NF-κB transcribes and regulates various inflammation-related genes, such as TNF-α, IL-1β and IL-6 cytokines and inflammatory mediators, such as leukotrienes, prostaglandins and chemokines, leading to an inflammatory response in neurons and glial cells. NF-κB activation can result in neuronal apoptosis, potentially leading to cognitive impairment and neurodegenerative diseases.

Cell-cell communication, including paracrine and autocrine signal transmission, is fundamental in neuroendocrine and immune regulation systems. Autocrine signaling contributes to the growth, differentiation, and maturation of immune cells, while paracrine communication is vital for immune cell recognition, aggregation, adhesion and phagocytosis (46).

Aforementioned, cytokine receptors such as CCR5, PTPRC, ITGB2, and FcRIIB serve roles in the pathological process after TBI (47,48). Most of these receptors receive paracrine signals from adjacent cells. The present analysis demonstrated that microglia and macrophages receive paracrine signals from neurons, astrocytes, endothelial cells and pericytes. These signals primarily activate the CCL and CX3C signaling pathways, directing leukocytes to aggregate at inflammation sites. Chemokines like CCL, which attract monocytes and macrophages, not only serve a chemotactic function but also provide signals for immune cell maturation. CX3C recruits T lymphocytes and neutrophils, and activates them to initiate immune responses (49). Furthermore, the TNF-α and TGF-β signaling pathways synergistically contribute to this process, impeding cell regeneration and inducing apoptosis. TNF-α, a key pro-inflammatory cytokine, is involved in vasodilation, edema formation and leukocyte adhesion to epithelia through the expression of adhesion molecules (50,51). It also regulates blood coagulation, induces oxidative stress at inflammation sites and indirectly causes cell death (52). TGF-β, a multifunctional cytokine prevalent in the nervous system, serves a vital role in repairing damaged neural tissues. It promotes growth, proliferation, migration and differentiation of neurons and glial cells and activates microglia, contributing to inflammation in the neural system.

While the present study has yielded valuable insights, it also faced certain limitations. Firstly, animal and clinical trials were not performed, limiting the depth of understanding of the role of TYROBP in living organisms. Although the present study predicted the upstream and downstream signaling pathways of TYROBP, it only assessed the role of the downstream NF-κB signaling pathway. Consequently, the assessment of the regulatory network mechanisms of TYROBP remains incomplete. Additionally, there is limited research on the development of drugs or interventions targeting TYROBP. Future studies should aim to address these limitations to more comprehensively and accurately understand the role of TYROBP in TBI and neuroinflammation and to support the development of potential treatments.

In conclusion, microglia serve a critical role in CNS damage and recovery after TBI. TYROBP is essential in microglial activation and is directly linked to neuronal cell death. These findings enhance understanding of the mechanisms of neuroinflammation caused by TBI and provide crucial references for further exploration of related treatments and interventions.

Acknowledgements

Not applicable.

Funding

This work was funded by the National Natural Science Foundation of China (grant nos. 82071465 and 81571283), the Sanming Project of Medicine in Shenzhen (grant no. SZSM201911007), the Natural Science Foundation of Shandong (grant no. ZR2020MH154), and the Key Project of Research and Development of Shandong Province (grant no. 2018GSF118215).

Availability of data and materials

The datasets used and/or analyzed during the current study are available from the corresponding author on reasonable request. Additionally, the high-throughput sequencing data was downloaded from the Gene Expression Omnibus (https://www.ncbi.nlm.nih.gov/geo/) with accession numbers; GSE71846, GSE180811, GSE192979, GSE173975, GSE173431, GSE167459, GSE163415, GSE144193, GSE129927, GSE79441, GSE180862, GSE160763 and GSE101901 (Table SII).

Authors' contributions

XZ was responsible for writing the article and, analyzing and interpreting the data. HS performed the single-cell data analysis. JH managed data collection, analysis and interpretation. WH is responsible for executing algorithms and statistics. QL conceived and designed the study. All authors have read and approved the final manuscript. ZX and QL confirm the authenticity of all the raw data.

Ethics approval and consent to participate

Not applicable.

Patient consent for publication

Not applicable.

Competing interests

The authors declare that they have no competing interests.

References

1. GBD 2016 Traumatic Brain Injury and Spinal Cord Injury Collaborators: Global, regional, and national burden of traumatic brain injury and spinal cord injury, 1990-2016: A systematic analysis for the Global Burden of Disease Study 2016. Lancet Neurol 18: 56-87, 2019.
2. Howlett JR, Nelson LD and Stein MB: Mental health consequences of traumatic brain injury. Biol Psychiatry 91: 413-420, 2022.
3. Sharp DJ, Scott G and Leech R: Network dysfunction after traumatic brain injury. Nat Rev Neurol 10: 156-166, 2014.
4. Kenney K, Amyot F, Haber M, Pronger A, Bogoslovsky T, Moore C and Diaz-Arrastia R: Cerebral vascular injury in traumatic brain injury. Exp Neurol 275: 353-366, 2016.
5. Corps KN, Roth TL and McGavern DB: Inflammation and neuroprotection in traumatic brain injury. JAMA Neurol 72: 355-362, 2015.
6. Maas AIR, Menon DK, Manley GT, Abrams M, Åkerlund C, Andelic N, Aries M, Bashford T, Bell MJ, Bodien YG, *et al*: Traumatic brain injury: Integrated approaches to improve prevention, clinical care, and research. Lancet Neurol 16: 987-1048, 2017.
7. Devanney NA, Stewart AN and Gensel JC: Microglia and macrophage metabolism in CNS injury and disease: The role of immunometabolism in neurodegeneration and neurotrauma. Exp Neurol 329: 113310, 2020.
8. Zhang ZW, Liang J, Yan JX, Ye YC, Wang JJ, Chen C, Sun HT, Chen F, Tu Y and Li XH: TBHQ improved neurological recovery after traumatic brain injury by inhibiting the overactivation of astrocytes. Brain Res 1739: 146818, 2020.
9. Tang B, Song M, Xie X, Le D, Tu Q, Wu X and Chen M: Tumor necrosis factor-stimulated gene-6 (TSG-6) Secreted by BMSCs regulates activated astrocytes by inhibiting NF-κB signaling pathway to ameliorate blood brain barrier damage after intracerebral hemorrhage. Neurochem Res 46: 2387-2402, 2021.
10. Dinet V, Petry KG and Badaut J: Brain-Immune Interactions and Neuroinflammation After Traumatic Brain Injury. Front Neurosci 13: 1178, 2019.
11. Takahashi H, Klein ZA, Bhagat SM, Kaufman AC, Kostylev MA, Ikezu T and Strittmatter SM: Alzheimer's Disease Neuroimaging Initiative: Opposing effects of progranulin deficiency on amyloid and tau pathologies via microglial TYROBP network. Acta Neuropathol 133: 785-807, 2017.
12. Castranio EL, Mounier A, Wolfe CM, Nam KN, Fitz NF, Letronne F, Schug J, Koldamova R and Lefterov I: Gene co-expression networks identify Trem2 and TYROBP as major hubs in human APOE expressing mice following traumatic brain injury. Neurobiol Dis 105: 1-14, 2017.
13. Haure-Mirande JV, Audrain M, Ehrlich ME and Gandy S: Microglial TYROBP/DAP12 in Alzheimer's disease: Transduction of physiological and pathological signals across TREM2. Mol Neurodegener 17: 55, 2022.
14. Haure-Mirande JV, Wang M, Audrain M, Fanutza T, Kim SH, Heja S, Readhead B, Dudley JT, Blitzer RD, Schadt EE, *et al*: Integrative approach to sporadic Alzheimer's disease: Deficiency of TYROBP in cerebral Aβ amyloidosis mouse normalizes clinical phenotype and complement subnetwork molecular pathology without reducing Aβ burden. Mol Psychiatry 24: 431-446, 2019.
15. Darwent L, Carmona S, Lohmann E, Guven G, Kun-Rodrigues C, Bilgic B, Hanagasi H, Gurvit H, Erginel-Unaltuna N, Pak M, *et al*: Mutations in TYROBP are not a common cause of dementia in a Turkish cohort. Neurobiol Aging 58: 240.e1-240.e3. 2017.
16. Siebold L, Obenaus A and Goyal R: Criteria to define mild, moderate, and severe traumatic brain injury in the mouse controlled cortical impact model. Exp Neurol 310: 48-57, 2018.

17. Leek JT, Johnson WE, Parker HS, Jaffe AE and Storey JD: The sva package for removing batch effects and other unwanted variation in high-throughput experiments. Bioinformatics 28: 882-883, 2012.
18. Ritchie ME, Phipson B, Wu D, Hu Y, Law CW, Shi W and Smyth GK: Limma powers differential expression analyses for RNA-sequencing and microarray studies. Nucleic Acids Res 43: e47, 2015.
19. Zhou Y, Zhou B, Pache L, Chang M, Khodabakhshi AH, Tanaseichuk O, Benner C and Chanda SK: Metascape provides a biologist-oriented resource for the analysis of systems-level datasets. Nat Commun 10: 1523, 2019.
20. Langfelder P and Horvath S: WGCNA: An R package for weighted correlation network analysis. BMC Bioinformatics 9: 559, 2008.
21. Wilkerson MD and Hayes DN: ConsensusClusterPlus: A class discovery tool with confidence assessments and item tracking. Bioinformatics 26: 1572-1573, 2010.
22. Qiu X, Mao Q, Tang Y, Wang L, Chawla R, Pliner HA and Trapnell C: Reversed graph embedding resolves complex single-cell trajectories. Nat Methods 14: 979-982, 2017.
23. Hao Y, Hao S, Andersen-Nissen E, Mauck WM III, Zheng S, Butler A, Lee MJ, Wilk AJ, Darby C, Zager M, *et al*: Integrated analysis of multimodal single-cell data. Cell 184: 3573-3587.e29, 2021.
24. Jin S, Guerrero-Juarez CF, Zhang L, Chang I, Ramos R, Kuan CH, Myung P, Plikus MV and Nie Q: Inference and analysis of cell-cell communication using CellChat. Nat Commun 12: 1088, 2021.
25. Liu N, Li Y, Jiang Y, Shi S, Niamnud A, Vodovoz SJ, Katakam PVG, Vidoudez C, Dumont AS and Wang X: Establishment and application of a novel in vitro model of microglial activation in traumatic brain injury. J Neurosci 43: 319-332, 2023.
26. Sachse F, Becker K, Basel TJ, Weiss D and Rudack C: IKK-2 inhibitor TPCA-1 represses nasal epithelial inflammation in vitro. Rhinology 49: 168-173, 2011.
27. Livak KJ and Schmittgen TD. Analysis of relative gene expression data using real-time quantitative PCR and the 2(-Delta Delta C(T)) method. Methods 25: 402-408, 2001.
28. Willis EF, MacDonald KPA, Nguyen QH, Garrido AL, Gillespie ER, Harley SBR, Bartlett PF, Schroder WA, Yates AG, Anthony DC, *et al*: Repopulating microglia promote brain repair in an IL-6-Dependent manner. Cell 180: 833-846.e16, 2020.
29. Wu H, Zheng J, Xu S, Fang Y, Wu Y, Zeng J, Shao A, Shi L, Lu J, Mei S, *et al*: Mer regulates microglial/macrophage M1/M2 polarization and alleviates neuroinflammation following traumatic brain injury. J Neuroinflammation 18: 2, 2021.
30. Krukowski K, Nolan A, Becker M, Picard K, Vernoux N, Frias ES, Feng X, Tremblay ME and Rosi S: Novel microglia-mediated mechanisms underlying synaptic loss and cognitive impairment after traumatic brain injury. Brain Behav Immun 98: 122-135, 2021.
31. Kennedy A, Waters E, Rowshanravan B, Hinze C, Williams C, Janman D, Fox TA, Booth C, Pesenacker AM, Halliday N, *et al*: Differences in CD80 and CD86 transendocytosis reveal CD86 as a key target for CTLA-4 immune regulation. Nat Immunol 23: 1365-1378, 2022.
32. Necula D, Riviere-Cazaux C, Shen Y and Zhou M: Insight into the roles of CCR5 in learning and memory in normal and disordered states. Brain Behav Immun 92: 1-9, 2021.
33. Al Barashdi MA, Ali A, McMullin MF and Mills K: Protein tyrosine phosphatase receptor type C (PTPRC or CD45). J Clin Pathol 74: 548-552, 2021.
34. Xu H, Zhang A, Han X, Li Y, Zhang Z, Song L, Wang W and Lou M: ITGB2 as a prognostic indicator and a predictive marker for immunotherapy in gliomas. Cancer Immunol Immunother 71: 645-660, 2022.
35. Verbeek JS, Hirose S and Nishimura H: The Complex association of FcγRIIb with autoimmune susceptibility. Front Immunol 10: 2061, 2019.
36. Konishi H and Kiyama H: Microglial TREM2/DAP12 Signaling: A Double-Edged sword in neural diseases. Front Cell Neurosci 12: 206, 2018.
37. Audrain M, Haure-Mirande JV, Mleczko J, Wang M, Griffin JK, St George-Hyslop PH, Fraser P, Zhang B, Gandy S and Ehrlich ME: Reactive or transgenic increase in microglial TYROBP reveals a TREM2-independent TYROBP-APOE link in wild-type and Alzheimer's-related mice. Alzheimers Dement 17: 149-163, 2021.
38. Zhou Y, Tada M, Cai Z, Andhey PS, Swain A, Miller KR, Gilfillan S, Artyomov MN, Takao M, Kakita A, *et al*: Human early-onset dementia caused by DAP12 deficiency reveals a unique signature of dysregulated microglia. Nat Immunol 24: 545-557, 2023.
39. Zhao N, Ren Y, Yamazaki Y, Qiao W, Li F, Felton LM, Mahmoudiandehkordi S, Kueider-Paisley A, Sonoustoun B, Arnold M, *et al*: Alzheimer's risk factors age, APOE genotype, and sex drive distinct molecular pathways. Neuron 106: 727-742, 2020.
40. Paradowska-Gorycka A and Jurkowska M: Structure, expression pattern and biological activity of molecular complex TREM-2/DAP12. Hum Immunol 74: 730-737, 2013.
41. Haure-Mirande JV, Audrain M, Ehrlich ME and Gandy S: Microglial TYROBP/DAP12 in Alzheimer's disease: Transduction of physiological and pathological signals across TREM2. Mol Neurodegener 17: 55, 2022.
42. Lanier LL and Bakker AB: The ITAM-bearing transmembrane adaptor DAP12 in lymphoid and myeloid cell function. Immunol Today 21: 611-614, 2000.
43. Peng Q, Malhotra S, Torchia JA, Kerr WG, Coggeshall KM and Humphrey MB: TREM2- and DAP12-dependent activation of PI3K requires DAP10 and is inhibited by SHIP1. Sci Signal 3: ra38, 2010.
44. Zhang L, Wei X, Wang Z, Liu P, Hou Y, Xu Y, Su H, Koci MD, Yin H and Zhang C: NF-κB activation enhances STING signaling by altering microtubule-mediated STING trafficking. Cell Rep 42: 112185, 2023.
45. Mecca C, Giambanco I, Donato R and Arcuri C: Microglia and aging: The role of the TREM2-DAP12 and CX3CL1-CX3CR1 Axes. Int J Mol Sci 19: 318, 2018.
46. Gyoneva S and Ransohoff RM: Inflammation after traumatic brain injury: therapeutic potential of targeting cell-cell communication by chemokines. Trends Pharmacol Sci 36: 471-480, 2015.
47. Joy MT, Ben Assayag E, Shabashov-Stone D, Liraz-Zaltsman S, Mazzitelli J, Arenas M, Abduljawad N, Kliper E, Korczyn AD, Thareja NS, *et al*: CCR5 Is a therapeutic target for recovery after stroke and traumatic brain injury. Cell 176: 1143-1157.e13, 2019.
48. Morris AB, Farley CR, Pinelli DF, Adams LE, Cragg MS, Boss JM, Scharer CD, Fribourg M, Cravedi P, Heeger PS and Ford ML: Signaling through the Inhibitory Fc Receptor FcγRIIB Induces CD8+ T Cell Apoptosis to Limit T Cell Immunity. Immunity 52: 136-150, 2020.
49. Pawelec P, Ziemka-Nalecz M, Sypecka J and Zalewska T: The impact of the CX3CL1/CX3CR1 axis in neurological disorders. Cells 9: 2277, 2020.
50. Younger D, Murugan M, Rama Rao KV, Wu LJ and Chandra N: Microglia receptors in animal models of traumatic brain injury. Mol Neurobiol 56: 5202-5228, 2019.
51. Blaser H, Dostert C, Mak TW and Brenner D: TNF and ROS Crosstalk in Inflammation. Trends Cell Biol 26: 249-261, 2016.
52. Meyers EA and Kessler JA: TGF-β family signaling in neural and neuronal differentiation, development, and function. Cold Spring Harb Perspect Biol 9: a022244, 2017.